Recent progress in the development of efficient biomass-based ORR electrocatalysts

Anthony Dessalle, Javier Quílez-Bermejo, Vanessa Fierro, Feina Xu, A. Celzard

Journal Pre-proof

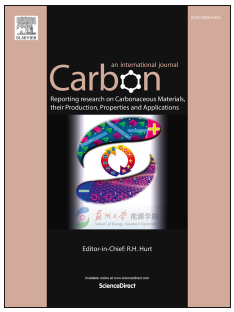

Recent progress in the development of efficient biomass-based ORR electrocatalysts

Anthony Dessalle, Javier Quílez-Bermejo, Vanessa Fierro, Feina Xu, Alain Celzard

PII: S0008-6223(22)00994-0

DOI: https://doi.org/10.1016/j.carbon.2022.11.073

Reference: CARBON 17713

To appear in: *Carbon*

Received Date: 25 August 2022

Revised Date: 10 November 2022

Accepted Date: 24 November 2022

Please cite this article as: A. Dessalle, J. Quílez-Bermejo, V. Fierro, F. Xu, A. Celzard, Recent progress in the development of efficient biomass-based ORR electrocatalysts, *Carbon* (2022), doi: https://doi.org/10.1016/j.carbon.2022.11.073.

Graphical abstract

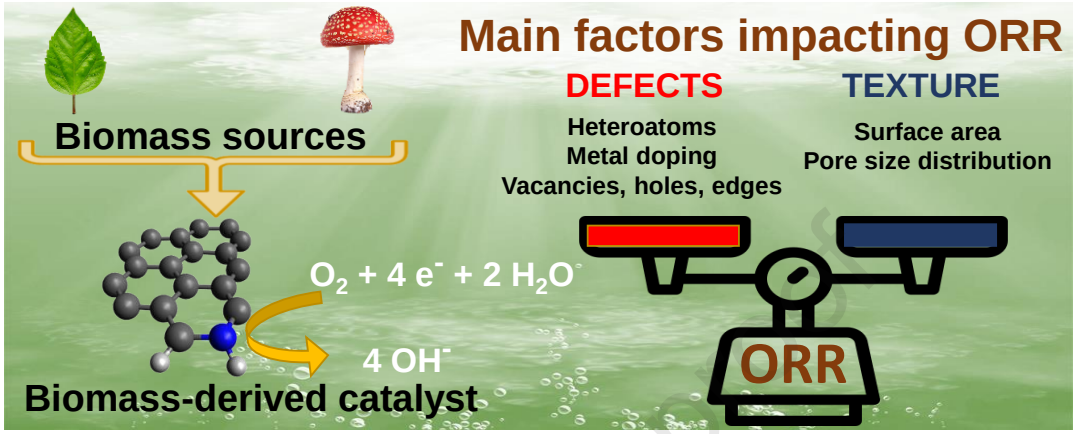

Recent progress in the development of efficient biomass-based ORR electrocatalysts

Anthony Dessalle[1,2], Javier Quílez-Bermejo[1,3], Vanessa Fierro[1], Feina Xu[2], Alain Celzard[1*]

[1] Université de Lorraine, CNRS, IJL, F-88000 Epinal, France

[2] Université de Lorraine, CNRS, LEMTA, F-54000 Nancy, France

[3] Universidad de Alicante, Departamento de Química Inorgánica and Instituto de Materiales, Ap. 99, 03080, Spain

[*] Corresponding author: Alain Celzard. E-mail: alain.celzard@univ-lorraine.fr

Abstract

Platinum is considered the reference catalyst in many electrochemical devices such as electrolyzers or fuel cells. Nevertheless, the large-scale commercialization of these Pt-based devices is limited by the prohibitive cost of platinum as well as its quantity and availability. Regardless of its price and scarcity, it is well known that the oxygen reduction reaction (ORR) with Pt in acidic media is slow compared to that in alkaline media. Due to the lower overpotentials in the latter case, the possibility of using Pt-free catalysts opens the door to new catalyst research. Among them, the development of carbon-based catalysts, either metal-free or with non-precious metals, from the conversion of biomass precursors by various synthetic processes has recently become a challenging goal, as biomass represents an eco-friendly source of carbon. The surface chemistry, textural properties and structure of carbonaceous materials make it complex to identify the origin of ORR catalytic activities. This review provides a critical discussion of the influence of the physicochemical and electrochemical properties of biomass-derived, carbon-based electrocatalysts for the ORR reported over the past decade.

Keywords: Oxygen reduction reaction; Biomass-derived carbon-based electrocatalysts; Metal-free catalysts; Non-precious metal catalysts; Pt-free electrocatalysts

Table of contents

Abbreviations

A_{BET}, BET area

BDS, benzyl disulfide

BET, Brunauer–Emmett–Teller

$C_{O_2}^b$, concentration of O_2 in the bulk of the electrolyte

CTAB, Cetyltrimethylammonium bromide

CV, Cyclic Voltammetry

DFT, Density Functional Theory

DMF, Dimethylformamide

D_{O_2}, diffusion coefficient of O_2 in the electrolyte

E_{ad}, adsorption energy of $HO_2^{\bullet}$

E_{ONSET}, onset potential

$E_{1/2}$, half-wave potential

HTC, Hydrothermal Carbonization

ICP, Inductively Coupled Plasma

j_k, kinetic current density

j_l, limiting current density

KL, Koutecky-Levich

LSV, Linear Sweep Voltammetry

MOF, Metal-Organic Framework

n, number of transferred electrons

NPMC, Non-precious metal-doped carbon material

OER, Oxygen Evolution Reaction

OMC, Ordered Mesoporous Carbon

OMS, Ordered Mesoporous Silica

ORR, Oxygen Reduction Reaction

PEMFC, Proton Exchange Membrane Fuel Cell

Pt/C, Platinum on Carbon

RDE, Rotating Disk Electrode

RHE, Reversible Hydrogen Electrode

RRDE, Rotating Ring Disk Electrode

SAC, Single-atom catalyst

ω, angular velocity

v, kinematic viscosity

1. Introduction

Excessive consumption of fossil resources, particularly to produce energy through the combustion of fossil fuels, leads to a significant increase in the amount of greenhouse gases, which are harmful to the planet, and is therefore at the heart of society's concerns about the acceleration of global warming. In order to reduce its impact, the Paris Agreement has set a maximum threshold of 1.5 °C increase in average temperature by the end of the 21st century [1]. To reach this target, it is imperative to change the current energy system by encouraging the development of new renewable energy sources.

Among possible renewable energy vectors, hydrogen is proposed as one of the most attractive alternatives to replace fossil fuels, as it can be used in fuel cells to produce electricity with water as the only byproduct. The most mature fuel cells that consumes hydrogen at the anode and oxygen at the cathode is the Proton Exchange Membrane Fuel Cell (PEMFC). This electrochemical device is a very promising because of the absence of polluting emissions and the high energy efficiency for energy production compared to combustion engines in vehicles that emit harmful exhaust gases (carbon monoxide, nitrogen dioxide, unburnt hydrocarbons, soot, heavy metals, etc.) [2]. Metal-air batteries emerge as other electrochemical systems being also widely studied to meet our growing energy needs. These systems generate electricity through electrochemical reactions on electrodes, which consist of a pure metal anode (e.g. lithium and sodium) and an ambient air cathode, which must exhibit efficient performance for the oxygen evolution reaction (OER) and the oxygen reduction reaction (ORR). The cathode electrode of metal-air batteries has significant drawbacks, such as large overpotentials for both reactions, high cost, and poor stability, which still need to be overcome to achieve greater efficiency in power generation [3,4].

The development of such technologies on a large scale is still limited due to the low kinetics and high overpotential of the ORR, which takes place at the cathode electrode of fuel cells and

metal-air batteries [5–7]. The sluggish kinetics of the ORR makes it necessary to use electrocatalysts to reduce the high overpotential of this reaction. Platinum is widely used because of its excellent performance as an ORR electrocatalyst, but its prohibitive price and low availability on Earth are a real bottleneck for fuel cell development [8]. To solve this problem, the design of low-cost electrocatalysts for ORR in alkaline and acidic media, with performance and stability close to that of platinum, is highly anticipated. Several strategies have been explored to replace platinum by designing: (i) metal-free carbon catalysts doped with heteroatoms, and (ii) non-precious metal electrocatalysts supported on carbon materials.

Biomass is the richest "green" source of carbon in nature, and it can be classified into three families: plant biomass (phytomass), animal biomass (zoomass) and microorganisms [5,9]. Every year, about 140 billion tons of biomass are generated worldwide and can be an environmental problem, especially in developed countries where most of biomass residues from agriculture are left in the fields to decompose [10,11]. To valorize biomass, one can first use it to produce energy, biofuels or biomaterials rich in heteroatoms (N, S, P, etc.) and metals (Fe, Cu, Mn, etc.) [12–14]. One can also use it for the production of carbonaceous materials that can be applied as electrocatalysts or as supports of metal active phases for ORR electrocatalysts [5,15–17]. Nevertheless, biomass precursors have inherently poor electrochemical properties, and therefore they must be modified or doped accordingly. The resulting materials can then exhibit unique textural properties, depending on the method of synthesis and the parameters used during the transformation of the biomass into carbonaceous materials (also known as chars) [10]. These chars have been shown to be of great interest in many applications such as energy storage and conversion (supercapacitors, batteries, fuel cells ...) [16].

Many interesting review articles have been published in recent years, providing important information on biomass-derived carbon-based electrocatalysts, with or without metals [5,15,18–20]. However, most of these papers focus on metal-free or metal-doped carbonaceous

catalysts from biomass by studying the influence of porosity or the influence of the chemical composition of these materials but rarely both combined. In this review, we propose to study both the impact of surface chemistry and textural properties on the ORR performance of several recently synthesized metal-doped and metal-free carbonaceous catalysts derived from biomass. The objective of the present paper is thus to provide a comprehensive overview of the performance of different ORR electrocatalysts based on biomass precursors synthesized during the past decade, with particular attention to the textural properties and chemical compositions of the carbon materials, including the identification of active sites. Below, the simplified mechanism of ORR on the surface of a carbon-based electrocatalyst in acidic or alkaline medium is first discussed, followed by a brief description of the most common biomass precursors and the synthesis strategies of biomass-based carbon materials. Next, a comparative study of heteroatom-doped carbon catalysts and non-precious metal-containing catalysts is discussed in detail, focusing on the effect of the biomass precursor and the consequences on ORR performance as a function of the textural properties and surface chemistry of the active sites.

2. Mechanism and kinetics of ORR

The mechanisms governing the oxygen reduction reaction (ORR) are based on a complex sequence of intermediate reactions. The most general and widely accepted mechanism in acidic medium (Figure 1) is that proposed by Wroblowa et al. [21]. Although it gives a simplistic view of the ORR, it is well known that it is highly dependent on the nature of the electrocatalysts and the working conditions.

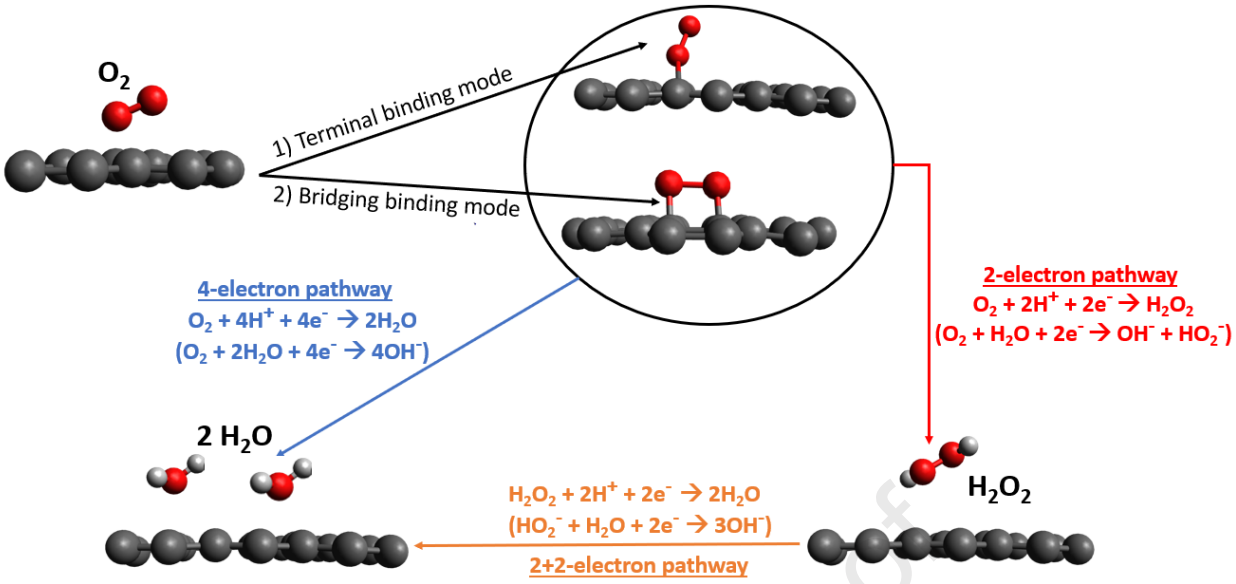

Figure 1. Simplified ORR mechanism on a carbon surface through three different pathways in acidic medium. The chemical reactions for ORR in alkaline medium are shown in brackets.

In general, the first step in the ORR in acidic medium is the chemisorption of O_2 molecules on the catalyst surface. They are then either reduced directly to water *via* the 4-electron pathway ($O_2 + 4\,H^+ + 4\,e^- \rightarrow 2\,H_2O$) or reduced to H_2O_2 *via* the 2-electron pathway ($O_2 + 2\,H^+ + 2\,e^- \rightarrow H_2O_2$). In the latter case, some materials may cause a further reduction of H_2O_2 to water molecules, leading to the 2+2-electron pathway ($H_2O_2 + 2\,H^+ + 2\,e^- \rightarrow 2\,H_2O$).

Another important issue is the method to be used to assess the catalytic activity for the ORR. Generally, the evaluation of the ORR performance of electrocatalysts is performed in a 3-electrode cell consisting of a working electrode, on which the electrocatalyst is deposited, a reference electrode and a counter electrode. The electrolytes used to study the oxygen reduction reaction can be alkaline (0.1 M KOH is the most commonly used) or acidic (typically 0.5 M H_2SO_4 or 0.1 M $HClO_4$) depending on the medium in which the electrocatalyst is to be characterized [2]. The influence of pH on the ORR activity of metal-free carbon-based catalysts has been studied previously. Experimental results showed that the ORR performance is worse in acidic than in alkaline media. According to DFT studies, this is due to a higher stabilization

of ORR intermediates in a protic environment, which leads to a higher energy requirement to complete the subsequent ORR steps and, consequently, to a lower catalytic activity [15]. The lack of protons in alkaline media leads to a lower stability of ORR intermediates and easy continuation of ORR mechanisms. It is worth noting that the ORR mechanisms in alkaline media are similar to those in acidic media (Figure 1). Nevertheless, H_2O_2 is converted into HO_2^- *via* equation (X1).

$$H_2O_2 + OH^- \rightarrow HO_2^- + H_2O \quad \text{(X1)}$$

The 4-electron pathway, the 2-electron pathway and the 2+2-electrons pathway are given in equations X2, X3 and X4, respectively.

$$O_2 + 2\,H_2O + 4\,e^- \rightarrow 4\,OH^- \quad \text{(X2)}$$

$$O_2 + H_2O + 2\,e^- \rightarrow OH^- + HO_2^- \quad \text{(X3)}$$

$$HO_2^- + H_2O + 2\,e^- \rightarrow 3\,OH^- \quad \text{(X4)}$$

Regardless of the medium in which the ORR occurs, the 4-electron pathway is generally preferred to the 2-electron or 2+2-electron pathway because of the absence of intermediate species (H_2O_2 or HO_2^-). The latter may indeed participate in undesirable reactions and accelerate the aging of certain electrochemical systems [22].

Cyclic voltammetry (CV) is often used to qualitatively evaluate the ORR electrocatalytic activity of materials by studying the position of the reduction peak in the cathodic scan in an O_2-saturated electrolyte. However, this route is insufficient to obtain accurate results due to the lack of quantitative parameters to compare different materials. At the same time, linear sweep voltammetry (LSV) with rotating disk electrodes (RDEs) aims to quantitatively study the kinetics of ORR by measuring several indicators such as onset potential, half-wave potential, limiting current density, or number of electrons transferred during the ORR process [23]. Figure 2 shows a typical linear sweep voltammetry (LSV) curve measured in a 3-electrode cell with

the presence of an electrocatalyst for ORR [24]. However, the definition and methods of determining these indicators differ among authors, and are generally not well explained or standardized. According to various publications in the literature, the most common definitions and determination methods for these indicators are as follows:

- The onset potential, E_{ONSET}, is the potential at which O_2 reduction begins, accompanied by an increase in current density. Some authors measure this potential at 5% of the limiting current density [25,26], while others take it at a fixed value of current density (*e.g.*, - 0.1 mA cm^{-2}) [27–29] .This parameter reveals important information about the kinetics of the ORR and is the most reported in the literature. In general, the standard catalyst used as a reference material in ORR is a commercial platinum-based electrocatalyst, with a 20 wt.% Pt loading supported on carbon black, here simply referred to as Pt/C. The measured onset potential for the commercial Pt/C is equal to or greater than 0.96 V vs. RHE in 0.1 M KOH solution, which may change slightly depending on the parameters used in the electrochemical measurements.

- The half-wave potential, $E_{1/2}$, is the potential corresponding to half the limiting current density. $E_{1/2}$ is then calculated as the intermediate value between the onset potential and the potential at which the diffusion-limited current is reached. For the commercial Pt/C, the half-wave potential is about 0.85 V vs. RHE in 0.1 M KOH solution.

- The limiting current density, j_l, is the measured current density at which the ORR is limited by mass transfer. This corresponds to the case where every molecule of O_2 arriving at the surface of the electrocatalyst is immediately reduced, and the current limitation comes solely from the diffusion of O_2 from the bulk of the electrolyte to the electrode surface and the number of electrons transferred.

- The number of transferred electrons can be defined as the number of electrons produced per molecule of O_2 reduced during the ORR process. Over the years, this parameter has been calculated by the Koutecky-Levich (KL) theory using Equation (1):

$$\frac{1}{j} = \frac{1}{j_k} + \frac{1}{j_l} = \frac{1}{j_k} + \frac{1}{0.62\, n\, F\, D_{O_2}^{2/3} C_{O_2}^{b} \nu^{-1/6}} \omega^{-1/2} \quad (1)$$

where j is the current density (A cm^{-2}) obtained after the normalization of the current measured during the experiment (A) by the geometric area of the electrode (cm^2), j_k is the kinetic current density (A cm^{-2}), j_l is the limiting current density (A cm^{-2}), ω is the angular velocity of the rotating electrode (rad s^{-1}), n is the number of transferred electrons, F is the Faraday constant (96 486.4 C mol^{-1}), D_{O_2} is the diffusion coefficient of O_2 in the electrolyte (cm^2 s^{-1}), $C_{O_2}^{b}$ is the concentration of O_2 in the bulk of the electrolyte (mol cm^{-3}), and ν is the kinematic viscosity of the electrolyte used (cm^2 s^{-1}). The inverse of the current ($1/j$) is then plotted against the inverse of the square root of the rotation speed ($\omega^{-1/2}$) to determine the number of electrons transferred (n) at different potentials [5,30].

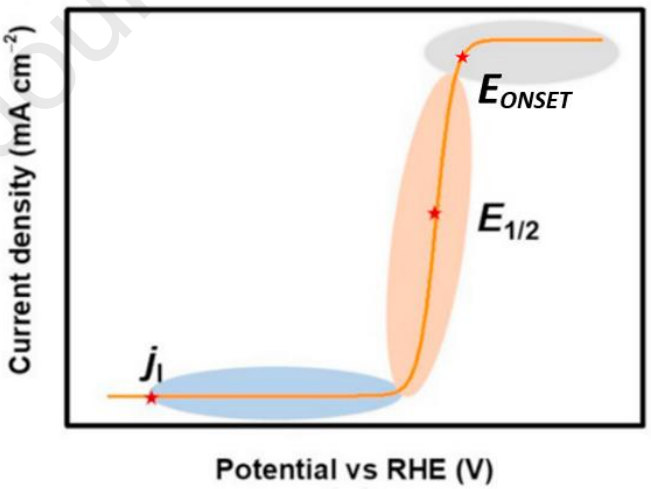

Figure 2. Schematic illustration of a linear sweep voltammetry (LSV) curve during ORR (Adapted from Ref. [24], Copyright 2021, with permission from Elsevier).

However, a recent publication has shown that the KL method is not accurate when using porous materials such as carbons [31]. This is because the KL theory was developed for a flat

surface and does not take into account the internal porosity. In this case, the use of the rotating ring disk electrode (RRDE) is more rigorous since the latter uses a second working electrode to quantify the amount of H_2O_2 generated during the ORR. The number of transferred electrons, *n*, is determined by measuring the currents produced on the disk (with the formation of H_2O_2 or HO_2^- in acidic and alkaline medium, respectively) and the current of the second working electrode with the oxidation of H_2O_2 or HO_2^-, again depending on the medium, to O_2 by applying a sufficiently positive potential on the ring, typically between 1.2 and 1.6 V vs. a reversible hydrogen electrode (RHE) (Equation (2)) [32]. This second working electrode is often based on a platinum ring, although gold has proven to produce even better results [33].

$$n = \frac{4I_d}{I_d + \frac{I_r}{N}} \quad (2)$$

In Equation (2), I_r (A) and I_d (A) are the measured currents at the ring and disk, respectively, and *N* is the RRDE collection efficiency (determined experimentally). The rate of H_2O_2 or HO_2^- (%) produced during the ORR process can also be calculated using Equation (3):

$$H_2O_2\ (\%) = 200\ \frac{NI_r}{I_d N + I_r} \quad (3)$$

3. Presentation of biomass and synthesis of an efficient electrocatalyst

3.1. Brief presentation of some biomasses

Biomass is the only component in nature that can be considered a green, inexpensive and abundant source of carbon. Furthermore, the unique properties of biomass make it an attractive precursor for the production of carbon materials with a variety of properties. The properties of these biomass-derived carbon materials depend on the nature, morphology, structure, textural properties, chemical composition, thermal history, etc., of the pristine precursor. This makes biomass and biomass-derived carbon chemistry a complex branch of science in which great

efforts have been made to advance the understanding of these materials in multiple applications, such as energy storage, sensing, environmental field or electrocatalysis, among others.

As mentioned above, biomass resources can be classified into three main categories [9,34]; (i) plant biomass (algae [35], seaweed [36,37], water hyacinth [38], alfalfa [39], seeds [40], straws [41,42], bagasse [43], etc.), (ii) animal and human waste biomass (bone [44,45], blood [25,46,47], urine [48], hair [49], tannery waste [50], etc.), and (iii) microorganisms (fungi [51–53], and bacteria [54–57]), as shown in Figure 3.

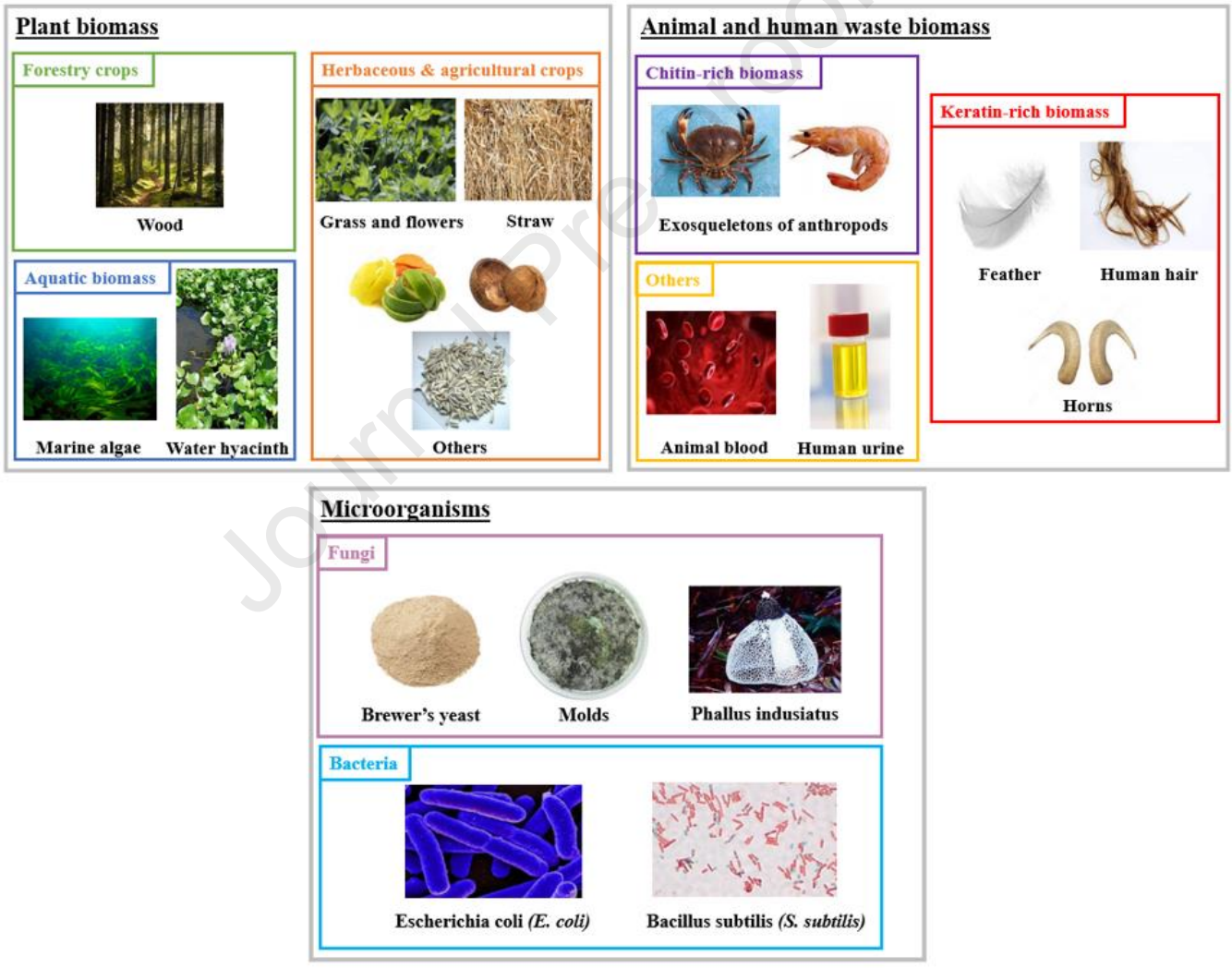

Figure 3. Presentation of some biomass sources used as catalyst precursors.

296 *3.1.1. Biomass of plant origin*

297 Cellulose, with the chemical formula $(C_6H_{10}O_5)_n$, is one of the main constituents of the cell
298 wall of many plants and is composed of several glucose units, the number of which depends on
299 its precursor. In general, cellulose is in the form of microfibrils with a parallel arrangement of
300 linear β-(poly-1,4-D-glucose) chains (Figure 4a). A collection of these microfibrils is called
301 cellulose fiber. Cellulose can also be synthesized by bacteria with a higher degree of
302 crystallinity and purity compared to that found naturally in plants, due to the absence of other
303 molecules that induce modifications and reduce the purity of plant cellulose [5,17,20,58,59].

304 The second most abundant biomass resource in nature is hemicellulose, which belongs to
305 the same polysaccharide family as cellulose. This polymer is composed of several sugar-based
306 units that consist of five-membered carbon heterocycles (xylose and arabinose), six-membered
307 carbon heterocycles (galactose and mannose) and seven-membered carbon heterocycles (4-O
308 methylglucuronic acid). These units are linked together through hydrogen bonds to form
309 hemicellulose (Figure 4b) [60]. The third most abundant plant biomass is lignin. Lignin is a
310 three-dimensional non-carbohydrate polymer composed of three phenylpropenoic alcohols
311 (coumaryl alcohol, coniferyl alcohol, sinapyl alcohol) that acts as a cement between cellulose
312 fibers, and making wood a cellulose-reinforced, lignin-matrix biocomposite to a first
313 approximation (Figure 4c) [20,61]. Finally, tannins are considered the fourth most common
314 plant biomass in nature. Tannins belong to the polyphenol family and are found in the vacuoles
315 and cell walls of plants, and are used as a chemical defense against several microorganisms,
316 insects and fungi [5,20,58,62]. Since the proportions of these different polymers vary from plant
317 to plant, the production of carbons from biomass results in a wide range of materials with
318 diverse physicochemical characteristics. However, carbohydrates and polysaccharides are
319 composed solely of carbon, oxygen and hydrogen atoms, which makes them unattractive
320 precursors of carbonaceous materials for obtaining highly efficient ORR electrocatalysts,
321 because the homogeneous distribution of charge density through the carbon layers is not

disrupted so that it can create active sites. To increase the catalytic properties of the resulting carbon materials, the introduction of heteroatoms is mandatory, as shown in the following references [5,63–65]. The introduction of N, P and S atoms indeed leads to a significant increase in the catalytic activity of glucose and lignin-derived carbon materials.

Other biomolecules of great interest for the production of carbons from biomass are carbohydrates. Carbohydrates are sugars that can be divided into three groups: (i) monosaccharides, which are composed of 3 to 7 carbon atoms (such as ribose with 5 carbon atoms or glucose with 6 carbon atoms), (ii) oligosaccharides, which are formed by 2 to 9 monosaccharides connected by glycosidic bonds (such as sucrose or maltose), and (iii) polysaccharides, which are macromolecules consisting of 10 or more monosaccharide units (such as starch) [66].

Agricultural biomass wastes and residues (crop leaves, roots, nut shells, fruit peels …) are therefore often useful as carbon precursors, as they are particularly rich in cellulose, hemicellulose and lignin [11]. Moreover, the forestry industry also generates significant amounts of biomass waste (sawdust, branches, etc.) that can be used to produce biomass-based carbon materials.

3.1.2. Biomass of animal and human origin

Animal and human biomass is mostly composed of proteins and minerals. Proteins are the most common animal biomass used to produce carbon materials. Proteins are macromolecules with a wide variety of polypeptides that are involved in multiple functions in living cells. One of the most interesting features of proteins for obtaining carbon materials is that they are based on nitrogen-rich compounds (from amino acid groups) and, therefore, they are interesting candidates for the preparation of nitrogen-doped carbon-based electrocatalysts [5].

Another important biomass precursor in the animal kingdom is chitin. With the formula $(C_8H_{13}O_5N)_n$, chitin is an amino-polysaccharide biopolymer found in fungi and the

exoskeletons of arthropods as ordered crystalline microfibrils (Figure 4d) [67]. Chitosan is a semi-crystalline polymer obtained when the deacetylation of chitin (removal of its acetyl group -CO-CH_3) approaches about 50% in alkaline medium (Figure 4d). Chitosan has unique complexing and chelating properties that will promote the incorporation of dopants into the resultant carbon material due to the presence of amino, hydroxyl and acetamido groups [68]. Keratin is also a promising precursor for the preparation of carbon materials derived from animal biomass. Keratin is a nitrogen- and sulfur-rich fibrous protein that is the main component forming the outermost layers of the vertebrates epidermis [69]. Keratin occurs primarily in two forms: α or β. The former is found in soft tissues (human air, sheep wool, etc.) while the latter is found in hard tissues (bird feathers, horns, hooves, etc.). Generally, keratin extraction is performed by acid, alkali or even enzyme hydrolysis of biomass precursors [70].

3.1.3. Microorganisms

Microorganisms are mainly divided into three families: fungi, bacteria and viruses. Among them, bacteria and fungi have attracted attention due to their rapid reproduction and special physicochemical properties [9]. They can be used as precursors and doping sources for the synthesis of carbon doped with one or more heteroatoms after decomposition and carbonization of proteins, phospholipids and metal salts [56,71]. Some metals such as iron can also be introduced into the carbon matrix originating from microorganisms [54,56].

Bacteria are considered the most common living organisms in natural environments. Typically, bacteria are grown in culture broths and then harvested after centrifugation, washing and drying [9]. During the transformation into carbonaceous material, the decomposition of polysaccharides, lipids and phospholipids present in bacteria allows the introduction of heteroatoms in the carbon skeleton such as nitrogen [54–56], phosphorus [54–56] or sulfur [54,56], which lead to the creation of numerous defects and active sites favorable to applications as catalysts.

Fungi are heterotrophic microorganisms that possess nuclei and cell walls. The main component of these walls is chitin [9,72], unlike plants where the main component is cellulose. Fungi can be divided into three types: molds [73], yeasts [74] and mushrooms [51–53]. They are distinguished by their differences in morphology and chemical composition of the cell wall. All fungi are rich in proteins and chitin, which will be used to obtain heteroatom doped-carbon materials, useful for application in electrocatalysis as in the case of bacteria [9].

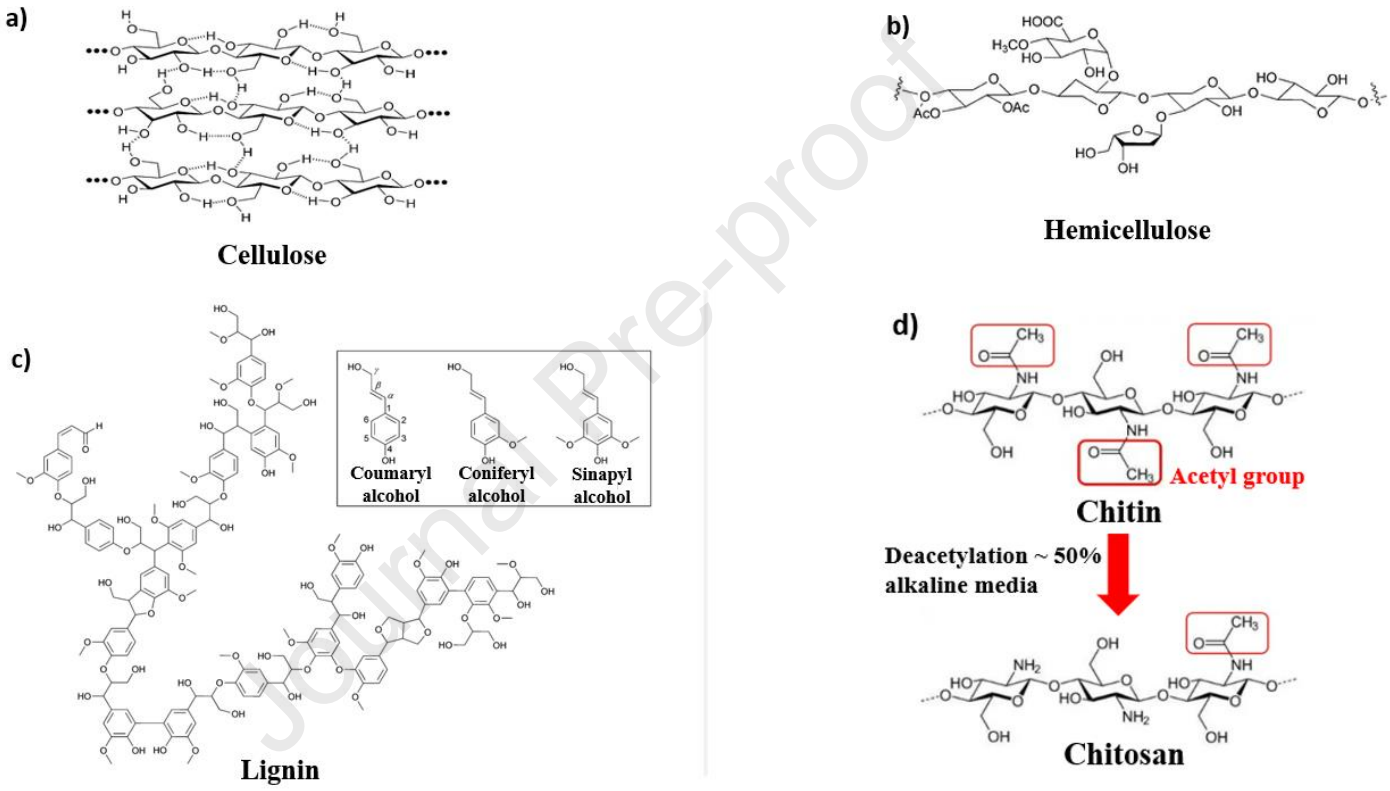

Figure 4. Chemical structure of: a) cellulose; b) hemicellulose; c) lignin; and d) chitin and chitosan.

3.2. Synthesis of carbon materials from biomass

Obtaining carbon materials from biomass depends on the multiple parameters of their possible synthesis methods, a summary of which is shown in Figure 5. The following is a brief overview of the most widely used and efficient techniques for the production of carbons from biomass. It should be emphasized that it is almost impossible to obtain undoped carbon

materials derived from biomass, as biomass is intrinsically rich in heteroatoms. It is possible to classify the different forms of heteroatom doping of the final products as: (i) intrinsic doping with heteroatoms coming from the constituent elements of the biomass precursor, or (ii) extrinsic doping where the heteroatoms have been intentionally introduced during the synthesis of the carbonaceous material.

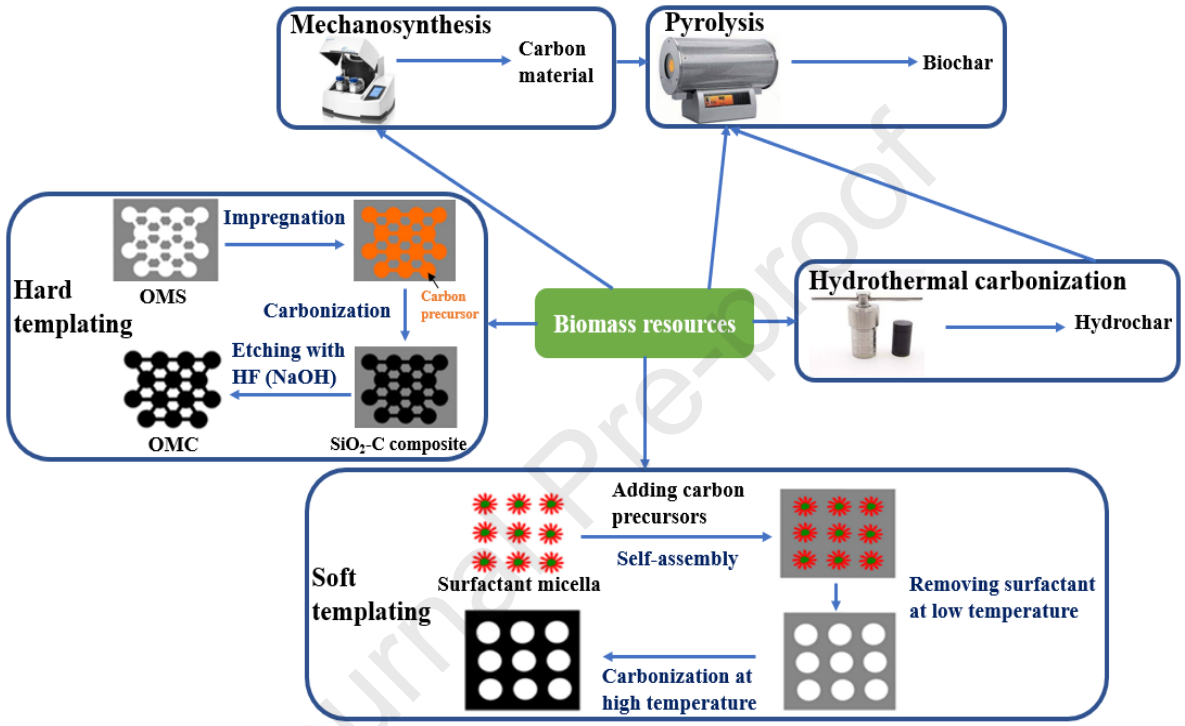

Figure 5. Conversion of biomass precursors into porous carbon materials by different synthesis routes. Hard-templating and soft-templating thumbnails (OMS and OMC standing for ordered mesoporous silica and carbon, respectively) are reprinted from Ref. [75], Copyright 2014, with permission from Elsevier.

3.2.1. Pyrolysis

Pyrolysis involves subjecting a carbonaceous precursor, *i.e.*, biomass in the present case, to thermal treatment at temperatures typically between 350 °C and 1000 °C, with a heating ramp of generally less than 10 °C min^{-1}, in an inert atmosphere, typically N_2 or Ar. The heating rate has a significant influence on the yield of carbon materials obtained from biomass. A high heating rate will lead to a low yield due to high volatilization of the precursor and bio-oils are

402 often obtained as the final product. In contrast, a high yield of carbon material (also called char)
403 can be obtained by using low heating rates [20].

404 The high temperatures of pyrolysis promote reactions in the precursor, such as condensation,
405 crosslinking, isomerization and dehydration reactions, which convert it into a carbon material.
406 In addition, various volatile compounds are released from the thermal decomposition of the
407 biomass. At low temperatures, the resulting material is mainly in the form of carbonaceous
408 materials with a high heteroatom content. This high degree of doping decreases when the
409 temperature of the thermal treatment increases, accompanied by a reorganization of the carbon
410 towards a less disordered state with a corresponding increase of the electrical conductivity [20],
411 but never going spontaneously to graphitization when the precursor is biomass. The presence
412 of certain metals, including Fe, Co, Ni and Mn, strongly influence the texture of the resulting
413 carbons, since these metals promote graphitization through the 2 to 5 electrons in the *d* atomic
414 orbitals that can induce strong bonds between the metal and the carbon-based materials [76].
415 Two possible mechanisms have been proposed for this catalysis process: (1) the dissolution-
416 precipitation mechanism where the amorphous carbon is first dissolved in metal particles and
417 then precipitates into graphitic carbon, and (2) the formation-decomposition mechanism of
418 intermediate carbides where the carbon interacts with the metal to produce metal carbides.
419 Then, the metal atoms in the metal carbide moieties are volatilized at high temperature, leaving
420 the graphitic carbon [10].

421 Activation is known as a process for improving or modulating the porosity and texture of
422 carbon materials by the action of an activating agent. This method can be used during the
423 pyrolysis of biomass to improve the textural properties of the resulting carbons. Physical
424 activation is defined as a controlled gasification of the material by the action of an oxidizing
425 gas with respect to carbon at the considered temperature, such as oxygen but especially water
426 vapor and carbon dioxide, used as reactive gases after a first step of pyrolysis under inert gas

427 [77]. On the other hand, chemical activation corresponds to the chemical attack by reagents in
428 the molten phase, such as $ZnCl_2$, KOH or NaOH [10,20,78]. Chemical activation is often
429 performed by impregnation or simple physical mixing of the biomass precursor with the
430 reagent. Then, a heat treatment is carried out. After cooling, the material is cleaned of excess
431 chemical agent by washing with water, and then filtered and dried [79]. Both chemical and
432 physical agents selectively attack the carbon material, generating a well-developed
433 micro/mesoporosity in the pristine carbon [80].

434 Furthermore, not only the activation of carbonaceous materials may be relevant, but also the
435 introduction of heteroatom precursors that can lead to the functionalization of biomass-derived
436 carbons. To achieve this goal, it is useful for the pyrolysis of the biomass precursor to occur in
437 the presence of one or more heteroatom sources (rich in nitrogen, sulfur, boron or/and
438 phosphorus) to allow the introduction of additional elements into the carbonaceous backbone
439 to change the electron and spin density around the surrounding carbon atoms. It is also common
440 to use a stream of NH_3 during pyrolysis to both add nitrogen to the material and create
441 micropores by reaction with carbon at high temperature, since ammonia acts as both an
442 activating and N-doping agent [5].

443 *3.2.2. Hydrothermal carbonization at low temperature*

444 Hydrothermal carbonization (HTC) is based on the reaction of a biomass precursor with
445 water in an autoclave at a temperature generally between 100 and 200 °C and under a self-
446 generated moderate pressure. The addition of an acid to the water accelerates the hydrolysis
447 and separation of the biomass components. The transformation of these components into gas
448 creates a large amount of micropores in the final carbonaceous material, usually called
449 hydrochar. In addition, the aqueous medium and low temperatures involved promote the
450 formation of a hydrochar with a large amount of oxygen functional groups, which decrease the
451 electrical conductivity of the material but improve its hydrophilicity [81]. The properties of

hydrochar depend not only on the HTC conditions, which are quite versatile since it is possible to vary the temperature, time, pressure, pH, concentration and nature of various additives, but also of course on the nature of the biomass itself. Falco et al. [82] proposed the hydrothermal carbonization of glucose and raw straw, leading to the production of monodisperse spherical particles in the case of the pure carbohydrate. For the lignocellulosic biomass, composed of a mix of biopolymers, a fibrous structure close to the initial structure of raw straw with some particles was obtained.

However, hydrochars generally have a much lower carbon content than carbon materials obtained directly by conventional pyrolysis due to the higher level of dehydration that takes place during pyrolysis. Moreover, the specific surface area and thus the pore volume are higher for carbonaceous materials obtained by pyrolysis than for hydrochars. This observation has been attributed to the residual presence of decomposition products on the surface of hydrochars, which implies pore blockage [83].

3.2.3. Mechanosynthesis

The aforementioned procedures for the preparation of carbon materials involve thermal treatments, which increases the cost of these methodologies. To overcome this limitation, mechanosynthesis has been proposed as a promising alternative to produce carbon-based materials by using mechanical forces to provide the energy needed to convert biomass into carbons. Mechanosynthesis is an advanced milling technique that consists of a solid-state powder processing technique [84]. In order to achieve reproducibility of the different syntheses, the use of ball mills is preferred as it provides control over the parameters (grinding speed and time) compared to the manual grinding with a mortar and pestle that is highly dependent on the user. During the rotation of the ball mill, collisions of the balls with the powders, through mechanical forces, induce bond cleavages and surface defects, leading to chemical modification of the reagents [85]. This is a new synthesis route for the preparation of carbonaceous materials,

whereas it has been widely used in recent years to obtain metal alloys and oxides.[86] Recent studies [87,88] have proven that the use of mechanosynthesis leads to carbon materials with high yield without the use of toxic and polluting solvents. Nevertheless, despite the high energy input of mechanosynthesis, a second pyrolysis step may be recommended for special applications in order to increase the degree of graphitization of the resulting carbon and thus the electrical conductivity of the material.

3.2.4. Template methods

One of the main limitations of pyrolysis and hydrothermal carbonization is the lack of control over the textural properties of the resulting carbon materials. In order to prepare carbon materials with controlled structures and porosities, the use of templates during thermal treatments is the most common methodology. Template methodologies can be classified into two different groups: hard-templating and soft-templating [89,90]. They are not strictly speaking methods for producing carbon materials but for modulating the textural properties of the resulting carbons. Templates can be used in pyrolysis, hydrothermal treatments and so on. Nevertheless, this section will explain the different types of templates and the advantages and disadvantages of their use.

The hard-template method is based on the replication of a well-structured material with a defined pore structure (such as mesoporous silicas [20,75,80], MOFs [78,91,92], zeolites [75,93], metal oxides [20] etc.). The carbon precursor is introduced into the pores of the template through chemical [94] or electrochemical [95] methods, and then heat treatment is applied. In hard-template methods, the template material is thermodynamically stable at high temperature and the carbon material is produced with the reverse structure of the template. Finally, the template can be removed, if required, using chemicals (*e.g.*, HF or NaOH). The main limitation of this method is indeed the use of such toxic chemicals for template removal, which limits the environmental friendliness of this type of carbon material production [20].

To avoid the major limitation of hard-template methods, soft-templating is proposed to overcome the use of hazardous chemicals. The soft-template method is based on the self-assembly of carbon precursors with amphiphilic molecules such as surfactants (*e.g.*, cetyltrimethylammonium bromide, CTAB [96]) or block copolymers (*e.g.*, Pluronic® F127 [87,88,97]) in a suitable solvent. Typically, the carbon precursor positions itself around the micelles spontaneously formed by the organic agents in the solution. The soft template is then removed during pyrolysis, leading to a developed but highly controlled porosity in the resulting carbon materials [20]. Other synthesis routes for the preparation of carbon materials exist, such as laser-induced carbonization [98] or microwave-assisted carbonization [99,100], which are notably used for the rapid heating of biomass, but they have not been widely discussed in the literature and only a few works can be found on these methods.

4. Biomass-derived carbon materials used in ORR

4.1. Metal-free, heteroatom-doped carbon materials

Biomass-derived carbon, whether intentionally doped or not, have been presented as one of the most promising alternatives as electrode materials in many applications, such as metal-air batteries [101], supercapacitors [79,102] or fuel cells [15]. The carbon precursor, the preparation method or the use of functionalization routes make biomass-derived carbons catalytically active materials or metal catalyst supports for ORR. Interestingly, heteroatoms, such as phosphorus, boron, and in particular nitrogen, play a prominent role in enhancing the ORR properties of carbon materials because they have an electron-withdrawal effect on the adjacent carbon atoms. This creates a positive electron density in the carbon network, which acts as an active site where dioxygen molecules are attracted, chemisorbed and then reduced [103–105]. In addition, heteroatoms can also serve as anchor points for various metals that can

also behave as active sites for the ORR. Since the strength of the metal-heteroatom bond is often much higher than the metal-carbon interaction, the activity and stability of heteroatom-based electrocatalysts are much higher than those of electrocatalysts that do not have such defects [19].

In general, defects located in the carbon matrix allow to generate active sites for the ORR, especially due to the presence of heteroatoms from the biomass precursor. Nevertheless, it should not be overlooked that the introduction of these heteroatoms also induces point defects that may also be responsible for the improved ORR performance of these electrocatalysts [63]. Whatever the nature of the heteroatoms concerned, it is possible to perform a mono-doping with a single heteroatom or a multi-doping in order to play on the synergy between several kinds of heteroatoms to increase the performances of the ORR [106]. From a theoretical and experimental points of view, the defects induced have been shown to be responsible for the high catalytic performance of different heteroatom-doped carbon materials. Among them, the role of pentagons and carbenes should be noted [107].

Textural properties should not be forgotten when considering active sites in carbon materials as it has been also shown that the higher the textural properties, the higher the catalytic activity towards the ORR. This is particularly notable when carbon materials have ultramicropores (pore width < 0.7 nm), which can act as “nano-reactors” that enhance the kinetics of this reaction [108,109]. Through mathematical modeling of the ORR in porous carbon materials, Gabe et al. [110] highlighted the importance of microporosity in facilitating the access of O_2 to active sites. In addition, they demonstrated that pore size distribution is of paramount importance by showing that narrow pores increase the residence time of the H_2O_2 molecules produced *via* the 2-electron pathway. This large residence time increases the chances of further reduction of H_2O_2 to water molecules *via* the 2+2-electron pathway.

The specific surface area of the synthesized biomass-based carbon material thus has a significant effect on the catalysis of the ORR by providing greater accessibility to the active sites. Usually, the specific area of a sample is determined by the well-known Brunauer–Emmett–Teller (BET) method, which consists in determining the nitrogen adsorption isotherms at -196°C and/or CO_2 at 0°C. The analysis of these isotherms then gives access to the textural properties of the material. The higher the available surface area, the greater the exposure of the active sites, resulting in improved catalytic performances in the ORR. Li et al. [111] prepared a biomass-derived N-doped carbon material by a two-step pyrolysis at 500 °C of *Scindapsus*-type aquatic plant under N_2 flow and then at 800 °C under NH_3. The resulting carbon material had a specific BET area of 1599 $m^2\ g^{-1}$ with an interconnected porous architecture favoring the transport of molecules to the active sites. This resulted in an excellent E_{ONSET} of 0.995 V vs. RHE and an $E_{1/2}$ of 0.825 V vs. RHE.

The porosity of carbon materials is not only due to the inherent characteristics of the precursors, but can also be modulated by the activation process, as discussed in Section 3.2. The use of chemical or physical agents in the thermal treatment of biomass precursor allows the generation of nanopores after the volatilization of several gases (H_2, H_2O, CO, CO_2, etc.) during pyrolysis, which has led to improved ORR activities in different carbon materials. Zhou et al. [112] thus obtained a biochar with a high specific area of 1969 $m^2\ g^{-1}$ after immersing eggplant pieces in a 0.5 M KOH solution for 24 hours, followed by pyrolysis at 800 °C. Then, the material was washed to remove excess KOH and the powder was ball-milled and subsequently heat-treated at 1000 °C in the presence of NH_3. The same synthesis was performed without KOH activation for comparison and the resulting surface specific area was 289 $m^2\ g^{-1}$ lower, resulting in a decrease in E_{ONSET} and $E_{1/2}$ of 90 mV and 200 mV, respectively. Other authors also used KOH [113–115] or $KHCO_3$ [115] as chemical activating agents to modify the textural properties and induce changes in microporosity to increase the electrocatalytic activity

in ORR of their biomass-based materials. Therefore, the specific surface area and the presence of different types of pores are important factors that influence the mass transport of O_2 to the active sites of the electrocatalyst and thus the kinetics of the ORR. Mesopores and macropores provide transport channels for dioxygen molecules to the active sites in the micropores and help the transport of water produced in the micropores to the bulk of the electrolyte.

However, having a large surface area does not always mean exhibiting excellent ORR activity. For example, He et al. [116] obtained an N, S co-doped carbon material with a specific surface area of 1689 $m^2 g^{-1}$ by a first pyrolysis at 800 °C of mulberry leaves as precursor in the presence of KOH, followed by a second pyrolysis in the presence of thiourea at the same temperature. However, they only obtained an onset potential of 0.86 V vs. RHE in alkaline medium. This proves that the specific surface area is important to provide good accessibility to the active sites but the nature and density of these sites are also relevant to induce the chemisorption and reduction of oxygen.

Nevertheless, this review article does not focus only on the textural properties of carbon materials and the consequences on catalytic activity for the ORR. If readers are interested in more information, we encourage them to read the works of Radovic [107,117] for an in-depth understanding of point defects and textural properties. In the following, we discuss the influence of biomass precursors and heteroatom composition on catalytic activity for the ORR.

4.1.1. Single heteroatom-doped carbon materials

4.1.1.1. Nitrogen-doped carbon materials

As commented above, carbonaceous materials produced from biomass are inherently rich in heteroatoms. This results in a change in electron density near the carbon atoms, which facilitates O_2 adsorption and charge transfer and thus improves ORR performance [63,118]. One of the origins of the controversy over N-doped carbon materials is the relationship between total nitrogen content and ORR activity. For many years, some authors [119,120] indeed directly

601 linked the catalytic activity towards ORR to the nitrogen content. Nevertheless, this claim has
602 been shown to be wrong because it is not only the N content that is relevant for ORR in N-
603 doped carbon materials, but more importantly the type of nitrogen. Zhang et al. [121] thus
604 reported the synthesis of a char obtained by mechanosynthesis of coconut shell powder,
605 melamine and $KHCO_3$ activator (introduced with a mass ratio of 1:3:3) followed by pyrolysis
606 at 800 °C. With a high nitrogen content (11.51 at.%) in their material, they obtained an E_{ONSET}
607 of 0.95 V vs. RHE and an $E_{1/2}$ of 0.77 V vs. RHE. Meanwhile, Wang et al. [122] produced a
608 biochar from coconut palm with only 2.84 at.% nitrogen but with better electrocatalytic
609 performance (E_{ONSET} = 1.01 V vs. RHE; $E_{1/2}$ = 0.87 V vs. RHE). This means that it is not the N
610 content that determines the ORR performance, but rather the nature of the nitrogen species that
611 must be additionally obviously accessible by the O_2 molecule in order to trigger the ORR
612 process.

613 The specific positions of the nitrogen atoms [123] (Figure 6a) in the carbon matrix appear to
614 play an important role in the catalytic activity towards the ORR. A general agreement seems to
615 be found after years of great controversy. For example, Zhang et al. [124] produced a nitrogen-
616 rich (4.26 at.%) carbonaceous material from Yuba with the majority in the form of graphitic N
617 (3.23 at.%), which shows a comparable electrocatalytic performance to commercial Pt/C with
618 an E_{ONSET} of 0.97 V vs. RHE and an $E_{1/2}$ of 0.86 V vs. RHE. The high proportion of graphitic
619 N in the material is reported to be the main reason for this high catalytic activity observed for
620 the ORR. The high catalytic performance of graphitic N was further confirmed by selective
621 doping of a carbon material [125,126]. The selective doping with a single species (i.e., graphitic
622 N) allowed the evaluation of the catalytic performance of such a functional group. Carbon
623 materials selectively doped with graphitic N showed similar catalytic performance to Pt/C
624 electrocatalysts, confirming the highly catalytic efficiency of this functionality towards the
625 ORR. In the work of Liu et al. [127], the proportion of pyridinic N and graphitic N is more than

626 50% of the total N content (7.76 at.%) detected in their carbonaceous material from water
627 lettuce, which could explain an E_{ONSET} equal to 1.00 V vs. RHE recorded for their catalyst.
628 Some other studies [111,128–133] have also shown that graphitic nitrogen (also called
629 quaternary) and pyridinic nitrogen are considered as the most active nitrogen species to provide
630 high catalytic performance for ORR activity compared to other nitrogen functionalities.
631 Nevertheless, some authors [134–137] have reported that pyrrolic nitrogen atoms or N-C-O
632 species have notable ORR catalytic activity.

633 The textural properties and degree of nitrogen functionalization have been shown to be very
634 important for the preparation of highly active N-doped carbon-based ORR electrocatalysts.
635 However, high degrees of functionalization often lead to a significant decrease in the porous
636 texture of carbon materials [138]. Figure 6b shows a graphical representation of nitrogen
637 content versus BET area for several biomass-derived N-doped carbon catalysts reported in the
638 literature [40,41,43,51,52,92,111–113,115,122,124,127,129–132,136,137,139–156]. This
639 graph indicates that the highest textural properties are observed in carbon materials with the
640 lowest degree of functionalization, and therefore, if a high nitrogen content is required, the
641 textural properties will likely be diminished. This was also observed in the work of Lin et al.
642 [157]. These authors increased the specific surface area of their N-doped carbon material by
643 increasing the proportion of KOH in the activation step: with the resulting increase in surface
644 area, the nitrogen content was significantly reduced. However, as discussed above, both
645 parameters are important for good catalytic properties in ORR. It is therefore imperative to find
646 the right balance between these two parameters to create a high-performance catalyst.

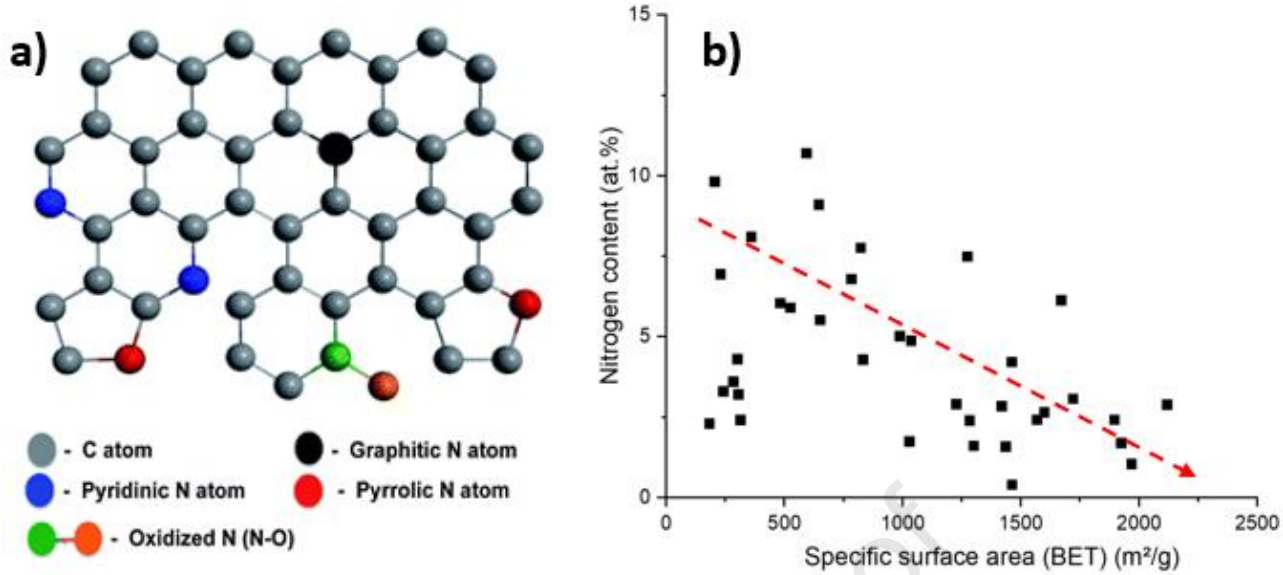

Figure 6. a) Possible positions of nitrogen atoms in the carbon backbone (Reprinted from Ref. [123] with permission from the Royal Society of Chemistry); b) Nitrogen content vs. specific BET area of different biomass-based N-doped carbon catalysts from the literature [40,41,43,51,52,92,111–113,115,122,124,127,129–132,136,137,139–156].

4.1.1.2. Sulfur-doped carbon materials

The introduction of other heteroatoms, such as sulfur, into biomass-derived carbon materials has also been studied due to the larger size of the sulfur atom, which not only induces changes in the electron density along the carbon layers, but also create additional defects in the carbon matrix. Sulfur-doped carbon spheres (4.04 at.% S) were obtained after solvothermal synthesis of sucrose with benzyl disulfide (BDS) and subsequent pyrolysis at 800 °C [158] (Figure 7a). The authors investigated the effect on the ORR performance of the S content by changing the sucrose/BDS molar ratio. The better catalytic performance was not attributed to the S content, but to the defects that were generated as a result of the addition of sulfur species during the heat treatment. High-temperature treatment indeed leads to the formation of S-based volatiles, resulting in a greater contribution of defects in the carbon material.

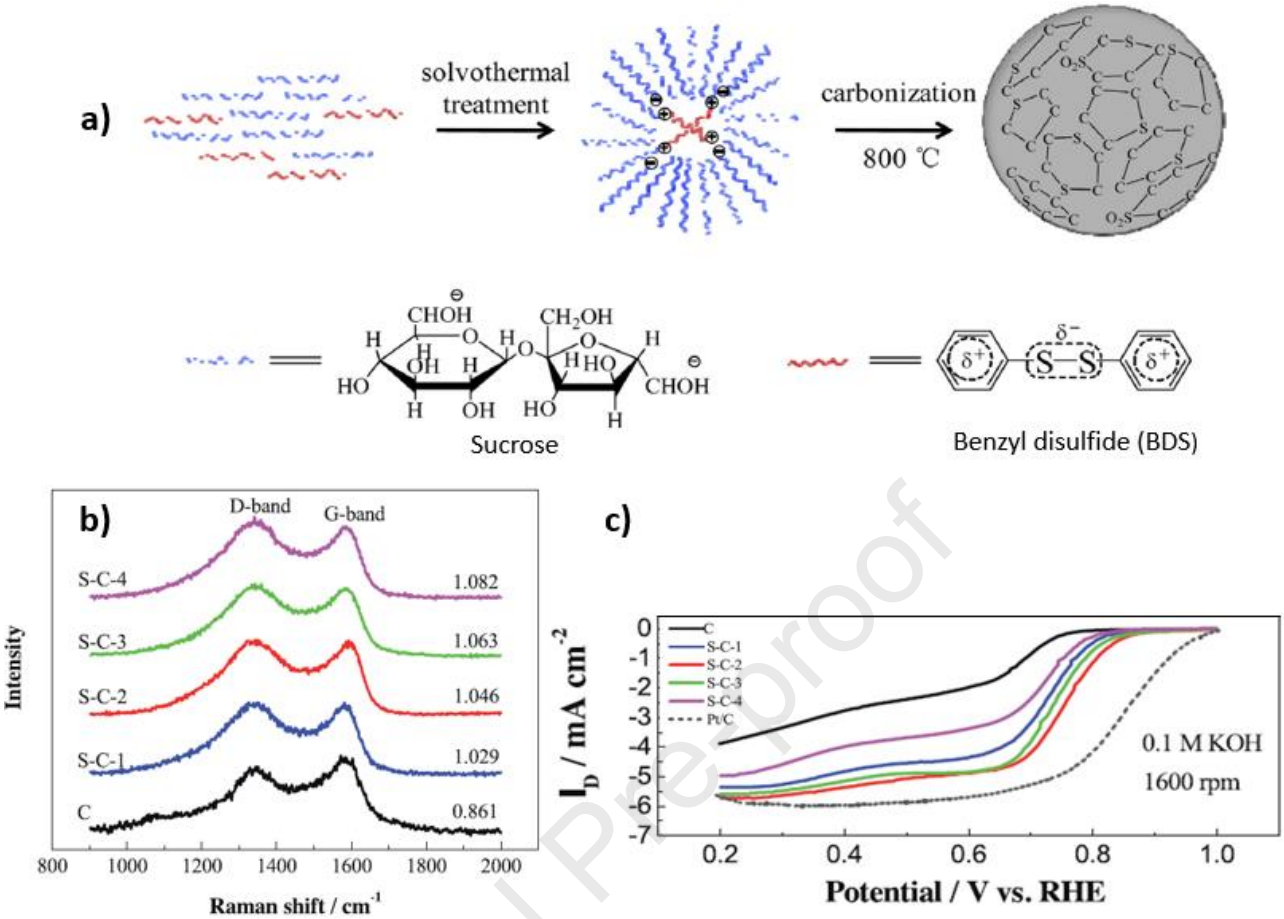

Figure 7. a) Schematic illustration of the preparation of S-doped carbon spheres; b) Raman spectra of as-prepared S-doped carbon spheres (S-C-1, S-C-2, S-C-3, S-C-4 refer to samples obtained with sucrose:BDS molar ratios of 10:1, 6:1, 4:1 and 1:1, respectively). The ratio of D-band to G-band (I_D/I_G) is given for each sample; c) Linear sweep voltammograms (LSVs) on the rotating ring-disk electrode for the as-prepared carbon spheres with and without S doping, and the commercial Pt/C catalyst in O_2-saturated 0.1 M KOH solution at 1600 rpm (Reprinted from Ref. [158], Copyright 2015, with permission from Elsevier).

To support this hypothesis, Raman spectroscopy was used as it provides valuable information about the structural order. With this technique, two characteristic peaks are observed in the spectra: the G-band and D-band, which are associated with stretching vibrations of the sp^2-hybridized C atoms and the defects in the carbon structure, respectively. The higher the I_D/I_G intensity ratio, the greater the presence of defects in general [159]. The sulfur-doped

samples showed a higher I_D/I_G ratio compared to pristine carbon (Figure 7b), suggesting that sulfur-doping has introduced additional defects. In addition, the S-doped carbon materials exhibited higher ORR catalytic performance than undoped carbon, indicating the importance of defects from the insertion of sulfur into the carbon backbone (Figure 7c).

Zhang et al. [160] performed DFT calculations to understand the nature of the active sites in sulfur-doped graphene. For the study, different clusters of sulfur-doped graphene were chosen: sulfur adsorbed on the graphene layer (Figure 8a), S-substitution at zigzag (Figure 8b) and armchair (Figure 8c) edges, SO_2-substitution at zigzag (Figure 8d) and armchair (Figure 8e) edges, and two pieces of graphene connected by sulfur ring clusters (Figure 8f). Based on the formation energy, sulfur adsorption on the graphene surface was found to be the most stable configuration and the presence of Stone-Walker defects enhance the sulfur doping. Moreover, the authors found that the active sites of these S-doped clusters are localized on the carbon atoms located at the zigzag edges or near the -SO_2 species. The electrocatalytic activity for ORR was attributed to the high spin and charge densities generated by these active sites.

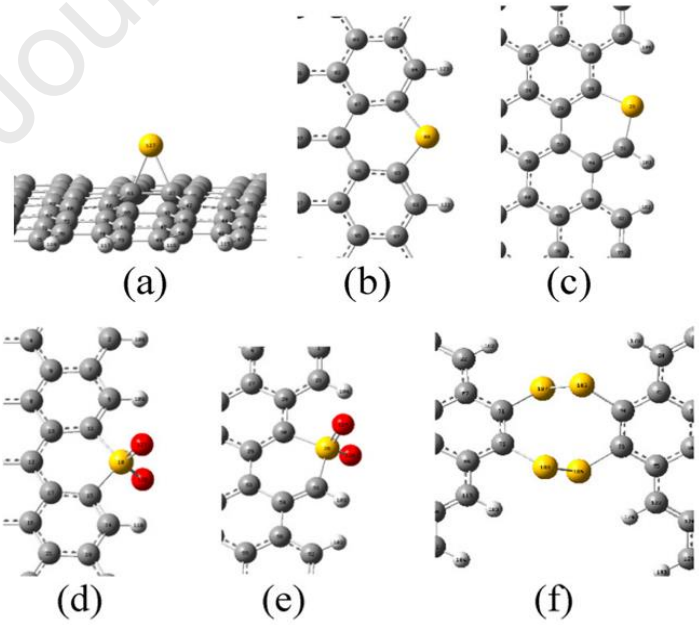

Figure 8. Illustration of several possible sulfur-doped graphene clusters: (a) sulfur adsorbed on the graphene layer; S-substitution at (b) zigzag, and (c) and armchair edges; SO_2-substitution

693 at (d) zigzag, and (e) armchair edges; and (f) two pieces of graphene connected by sulfur ring
694 clusters (f). Carbon, hydrogen, sulfur, and oxygen atoms are shown in gray, white, yellow and
695 red, respectively (Reprinted with permission from Ref. [160], Copyright 2014, with permission
696 from American Chemical Society).

697

698 *4.1.1.3. Phosphorus-doped carbon materials*

699 Heteroatoms less electronegative than carbon, such as phosphorus, have also been used to
700 facilitate the adsorption and reduction of the dioxygen molecule in carbon materials. The
701 creation of a positive charge on the phosphorus facilitates the chemisorption of O_2 directly onto
702 the heteroatom and not onto neighboring carbon atoms as was the case with nitrogen doping.
703 For instance, effective doping of hollow carbon spheres with homogenously distributed
704 phosphorus on the surface (1.59 at.%) and in the bulk (1.61 at.%) of the material was prepared
705 by Wu et al. [161] using tetraphenylphosphonium bromide as the phosphorus source and
706 glucose as the carbon source. They also used an anionic surfactant (sodium dodecyl sulfate) to
707 control the morphology and porosity of the final material obtained by hydrothermal synthesis
708 followed by pyrolysis at 800 °C. They attributed the high ORR performance (E_{ONSET} = 0.90 V
709 vs. RHE) to the phosphorus species, proposed as active sites, and/or to the modified electronic
710 density induced by the phosphorus species. The introduction of phosphorus into the carbon
711 matrix induces changes in the carbon atoms located near the P heteroatom, which might lead to
712 improved catalytic activity. DFT simulations were performed to study the influence of
713 phosphorus atoms on the ORR activity of P-doped carbon materials [162]. The presence of
714 phosphorus promotes O_2 chemisorption on the surface of P-doped graphene and CNTs. O_2
715 molecules bind in a bridging bond mode configuration on P atoms, forming two P-O bonds.
716 Subsequently, oxygen reduction occurs through dissociation of the dioxygen molecules into
717 two oxygen atoms or through hydrogenation with the formation of OOH species [162,163].

Although the origin of the catalytic activity of N-doped carbon materials seems clearer, the identification of the active sites in other heteroatom-doped carbons is controversial. Few researchers directly attribute catalytic activity to heteroatoms, but others link it to defects generated after volatilization of these species. Further understanding of this topic must be addressed in the coming years for the design of advanced metal-free carbon-based electrocatalysts. Table 1 reports the synthesis procedure, physicochemical properties and ORR performance obtained from some metal-free and single heteroatom-doped carbons derived from biomass.

Table 1. Metal-free and single heteroatom-doped carbon electrocatalysts for ORR. Electrochemical data were obtained in 0.1 M KOH electrolyte.

Biomass source	Other sources	Synthesis method	Doping atoms (at.%)	Specific surface area ($m^2\ g^{-1}$)	Total pore volume ($cm^3\ g^{-1}$)	E_{ONSET} (V vs. RHE)	$E_{1/2}$ (V vs. RHE)	j_l (mA cm^{-2}) at 1600 rpm	Number of transferred electrons *n*	Ref.
Scindapsus	NH_3	Pyrolysis	N: 2.65	1599	--	0.995	0.825	--	3.9	[111]
Eggplant	KOH NH_3	Activation, ball-milling, pyrolysis	N: 1.04	1969	--	0.93	0.83	5.5 at 0.2 V vs. RHE	3.87	[112]
Plum blossom	KOH Melamine	Carbonization, activation, pyrolysis	N: 2.89	2119	0.76	0.91	0.82	5.96 at 0.2 V vs. RHE	3.83	[113]
Papaya skin	Melamine $KHCO_3$	Pyrolysis, ball-milling, pyrolysis, activation	N: 6.13	1671	--	1.00	0.85	5.84 at 0.2 V vs. RHE	3.96	[115]
Coconut mesocarp	Melamine $KHCO_3$	Ball-milling, activation, pyrolysis	N: 11.55	1676	0.72	0.95	0.77	5.05 at 0.2 V vs. RHE	~4	[121]
Coconut palm leaves	Melamine KOH $KHCO_3$	Pyrolysis, functionalization, activation	N: 2.84	1419	0.94	1.01	0.87	5.5 at 0.2V vs. RHE	3.96	[122]
Glucose	Zeolitic imidazolate framework (ZIF-7)	Immersion, pyrolysis	N: 6.79	783	0.56	0.86	0.70	--	3.68	[92]
Corn starch	Urea	Immersion, pyrolysis	N: 2.42	1569	3.65	0.93	0.81	--	3.54-3.7	[129]

Yuba	$ZnCl_2$	Immersion, pyrolysis	N: 4.26	832	--	0.97	0.86	5.09 at 0.6 V vs. RHE	3.81	[124]
Water lettuces	NH_3	Freeze-drying, pyrolysis	N: 7.76	823	0.57	1.00	0.89	--	3.82-3.98	[127]
Shrimp shells	--	HTC, Silica templating, pyrolysis	N: 8.1	360	--	0.91	0.75	5.3 at 0.6 V vs. RHE	3.75-3.95	[131]
Soybean dregs	Urea	Calcination urea, pyrolysis	N: 6.04	483	1.57	0.90	0.77	--	3.31-3.63	[132]
Chicken feathers	KOH	Activation, pyrolysis	N: 4.3	301	--	0.96	--	--	--	[136]
Chicken feathers	KOH	Carbonization, activation, pyrolysis	N: 2.3	183	0.24	0.98	--	--	~4	[137]
Glucose	CNTs Urea	Immersion, pyrolysis	N: 10.7	594	0.58	0.95	0.82	--	3.9	[139]
Bacterial cellulose	Urea	Immersion, freeze-drying, pyrolysis	N: 9.82	206	--	0.93	0.80	5.0 at 0.4 V vs. RHE	3.6-4.0	[140]
Typha orientalis	NH_3	HTC, freeze-drying, pyrolysis	N: 9.1	898	0.36	0.93	0.78	4.8 at 0.2 V vs. RHE	3.85-3.96	[141]
Silk cocoons	$ZnCl_2$	Boiling, carbonization, activation	N: 7.49	1274	0.6	0.99	0.83	--	3.72-3.96	[142]
Bacterial cellulose	Polypyrrole	Polymerization, lyophilization, pyrolysis	N: 6.94	230	--	0.93	--	5.7 at 0.2 V vs. RHE	~4	[143]
Soybean	Na_2CO_3 $CaCl_2$	Immersion, boiling, coagulation, freeze-drying, pyrolysis	N: 5.52	652	0.68	0.94	0.81	4.41 at 0.4 V vs. RHE	3.48-3.84	[144]
Beancurd	NaCl Urea Na_2CO_3	Immersion, lyophilization, pyrolysis, immersion, pyrolysis	N: 5.02	988	0.69	0.96	0.81	--	3.9	[145]
Glucose	Dicyan-diamide $ZnCl_2$	HTC, activation	N: 4.88	1036	0.53	0.92	--	2.67 at 0.5 V vs. RHE	3.5-3.9	[146]
Corn straw	KOH	Carbonization, activation	N: 4.21	1461	0.92	0.81	--	--	--	[41]
Dandelion seeds	$ZnCl_2$	Activation, pyrolysis	N: 2.9	1228	0.67	0.83	0.75	4.98 at 0.1 V vs. RHE	3.7-4.0	[40]
Glucose	NH_3	HTC, pyrolysis	N: 2.61	2589	1.71	0.84	0.76	--	3.60-3.77	[148]

Enoki mushrooms (*Flammulina velutipes*)	CNTs	Ball-milling, pyrolysis	N: 3.2	305	0.35	0.94	0.81	3.98 at 0.5 V vs. RHE	3.9	[52]
Pomelo peels	--	HTC, pyrolysis	N: 2.41	314	0.22	0.88	--	--	3.52	[150]
Bagasse	NH_3	Boiling, freeze-drying, pyrolysis	N: 2.4	1284	--	0.88	0.77	5.21 at 0.1 vs. RHE	3.8	[43]
Grape skins	--	Fermentation, HTC, pyrolysis	N: 1.74	1029	0.52	0.96	--	6.93 at 0 V vs. RHE	3.8-4.0	[152]
Ginkgo leaves	NH_3	Pyrolysis, pyrolysis	N: 1.59	1436	--	--	0.81	--	3.7	[153]
Alder wood	NaOH Dicyandiamide	Activation, immersion, pyrolysis	N: 1.7	1924	1.6	0.93	0.8	--	~4	[154]
Poplar catkins	$ZnCl_2$	Activation, pyrolysis	N: 0.4	1463	1.31	0.82	0.76	--	~4	[155]
Lotus roots	K_2CO_3	Carbonization, ball-milling, activation	N: 1.61	1301	0.74	0.84	0.76	4.4 at 0.2 vs. RHE	~4	[156]
Sucrose	Benzyl disulfide	HTC, pyrolysis	S: 4.0	561	0.18	0.88	0.77	5.06 at 0.5 V vs. RHE	3.81	[158]
Glucose	$C_{24}H_{20}P(Br)$, sodium dodecyl sulfate	HTC, soft-templating, pyrolysis	P: 1.61	654	0.36	0.90	--	--	3.86	[161]

729

730 *4.1.2. Multi-doped carbon materials*

731 The purpose of doping with several heteroatoms is the creation of a synergistic effect in the
732 electron density of the carbon material to improve the catalytic activity for ORR, due to the
733 presence of different active sites or the coexistence of different moieties. Co-doping and multi-
734 doping of porous carbonaceous materials are very common in the literature as they allow
735 maximizing the effects produced by each heteroatom in the carbon structure [106]. This multi-
736 doping can be obtained from two alternative strategies: (i) the use of biomass precursors
737 containing different heteroatoms; or (ii) the introduction of external sources of heteroatoms into
738 the biomass precursors.

4.1.2.1. Nitrogen and sulfur co-doped carbon materials

One of the most interesting performances of co-doped carbon materials is achieved by the introduction of nitrogen and sulfur together. The work of Li et al. [164] showed a synergistic effect by the introduction of pyridinic and graphitic nitrogen species along with thiophene species into the carbon backbone. The authors attributed the coexistence of the two N and S heteroatoms as the responsible for the improved catalytic properties towards the ORR. Nevertheless, they also mentioned the presence of intrinsic defects in the carbon matrix that could explain this increase in ORR performance. In this sense, Radovic et al. [165] demonstrated that the presence of nitrogen and point defects in the vicinity can also improve the catalytic activity. Indeed, carbenes, carbynes or even H-deficient free radicals can be part of zigzag and armchair edges of graphene and catalyze the reduction of oxygen. Gao et al. directly carbonized sweet potato vine [166] and honeysuckle [167] at 800 °C to produce nitrogen- and sulfur-doped carbon materials. The biochar obtained from honeysuckle contained a higher proportion of N-pyridinic and S-thiophene species and, according to the authors' hypothesis, had better catalytic properties for the ORR compared to that obtained from sweet potato vine alone. Similarly, Amiinu et al. [168] attributed the ORR catalytic activity of their N, S-co-doped carbon material from the pyrolysis of graphene oxide with sheep horn due to the presence of a significant amount of graphitic N and pyridinic N with sulfur incorporated at the defect sites and edges in the form of thiophene species. The same conclusion was drawn by Zhang et al. [169] for their N,S-doped carbon material obtained from rapeseed. Density functional theory (DFT) has been applied by Liang et al. [170] to dual-doped nitrogen and sulfur carbon materials. It showed the presence of a large number of active carbon atoms due to the synergistic effect of S- and N-doping that introduces asymmetrical charge and spin densities, resulting in higher ORR performance (Figure 9a). The same kind of effect was also observed with B- and B,N-doping (Figure 9b, 9c).

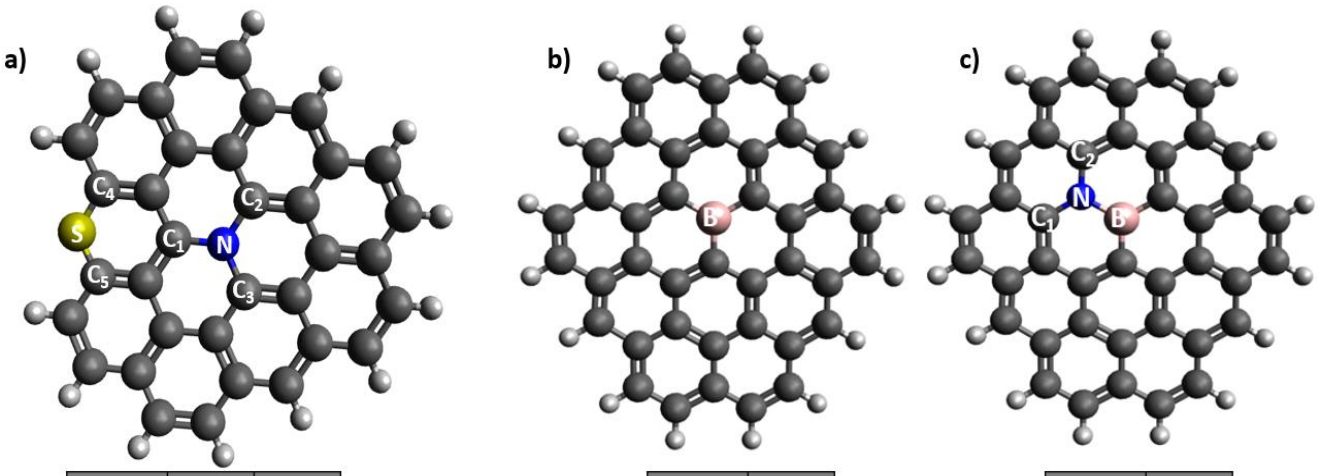

Atom Number	Spin density	Charge density
C1	0.43	0.23
C2	-0.03	0.28
C3	-0.03	0.28
C4	0.16	-0.22
C5	0.16	-0.22
N	0.06	-0.88
S	0.09	0.21

Atom Number	Charge density
B	0.10

Atom Number	Charge density
C1	0.69
C2	0.73
N	> 0
B	0.40

764

765 **Figure 9.** (a) Spin and charge density of the carbon network (C, black) in which nitrogen (N,
766 blue) and sulfur (S, yellow) are incorporated (Adapted from Ref. [170], Copyright 2012, with
767 permission from John Wiley and Sons); (b) Charge distribution of boron-doped graphene and
768 (c) B-doped graphene containing one graphitic nitrogen (Adapted from Ref. [171], Copyright
769 2019, with permission from Elsevier).

770 Most biomass precursors do not contain multiple heteroatoms in their chemical composition.
771 Therefore, external functionalization of biomass-derived carbon materials is a common strategy
772 to increase the catalytic activity towards the ORR. For example, Shen et al. [172] obtained an
773 onset potential of about 1.00 V vs. RHE in alkaline medium using S-containing lignin from
774 sugarcane residues with melamine and urea (external sources of nitrogen) initially dispersed in
775 dimethylformamide (DMF). The mixture was pyrolyzed at 1000 °C and the resulting carbon
776 materials showed a nitrogen content of 4.18 at.% (2.7 at.% of graphitic N) in the final product.
777 However, the authors did not attribute the highly efficient catalysis to the presence of S
778 moieties, but only to the graphitic N and total pore volume (1.40 cm^3 g^{-1}). There are multiple

routes to produce an N, S-doped carbon material. Other examples of preparing such materials are the simultaneous use of two heteroatom-containing precursors in the thermal treatment, such as methylene blue [173] or thiourea [116,174,175], both rich in N and S.

4.1.2.2. Nitrogen and phosphorus co-doped carbon materials

Co-doping carbon materials with nitrogen and phosphorus is another popular option for scientists because the synergy between these two heteroatoms provides high-performance electrocatalysts for ORR. For example, Wei et al. [55] synthesized an N, P-doped carbon material from the direct pyrolysis of *Escherichia coli* (*E. coli*) bacteria at 1000 °C for 2 h in an N_2 atmosphere. The authors attributed the very efficient electrochemical performance of their material in alkaline media (E_{ONSET} = 0.87 V vs. RHE, j_l = 6.21 mA cm^{-2} at 0.1 V vs. RHE) to the presence of a large proportion of pyridinic N, graphitic N and P-C bonds, highlighting a synergistic effect between N and P. Gao et al. [176] have identified by DFT simulation and experimentally verified that the active sites in N- and P-co-doped carbon materials are located at the edges of graphene layers, specifically near the oxidized P sites in the vicinity of graphitic nitrogen. The order of introduction of the N and P dopants appears to be of paramount importance according to Zhao et al. [177] When phosphorus is introduced first into the carbon lattice, it is either bound with a bridging mode configuration (outside mode, Figure 10a) or in substitution of a carbon atom in the matrix (inside mode, Figure 10b) causing the distortion of the 2D structure of the catalyst. The authors pointed out that if P is introduced by the inside mode, when N is subsequently introduced, it can replace P atoms in the carbon matrix (see Figure 10c), leading to a higher number of graphitic N atoms in the carbon material, known to be highly active sites for the ORR. The authors also demonstrated by DFT studies that the formation of graphitic N around phosphorus functionalities is thermodynamically favored.

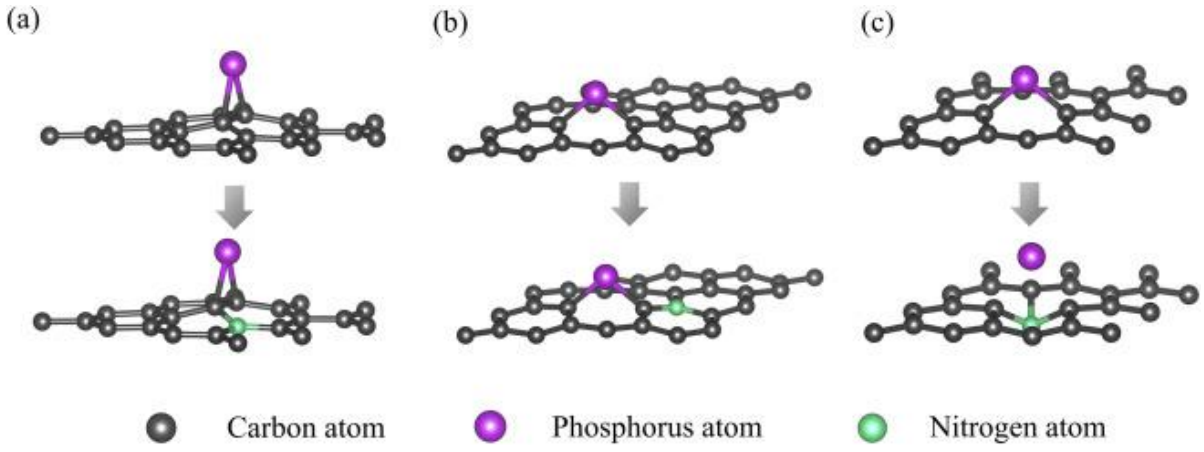

Figure 10. Representations of different doping modes when phosphorus is introduced first, and then nitrogen. (a) Outside mode; (b) inside mode; and (c) self-sacrifice mode (Reprinted from Ref. [177], Copyright 2018, with permission from Elsevier).

4.1.2.3. Nitrogen and boron co-doped carbon materials

Cao et al. [178] reported the synthesis of B,N-doped *Platanus*-based carbon material by impregnation of *Platanus* fruit hair in a solution of urea and boric acid (4:1:1 mass ratio), followed by pyrolysis at 900 °C under N_2. The authors attributed the effective ORR performance of the resulting carbon materials to the synergistic effect of N and B. The boron atom in B-C-N configuration retains a more positive charge density compared to the B-C configuration, resulting in a better adsorption step that subsequently leads to a better ORR performance. Zhang et al. [179] showed in their DFT calculations that the synergy between boron and nitrogen in an N, B-co-doped sample leads to a lower adsorption energy of the OOH· intermediate formed during ORR, compared to carbons doped only with nitrogen or boron (Figure 11a). Indeed, an increase of the charge density of the boron is observed when nitrogen surrounds it. They also showed that the ORR is particularly enhanced when the B-C-N functionalities are located at graphene edges. Based on the adsorption energies of the OOH· intermediate on N, B-doped carbon catalysts, they revealed that oxygen chemisorption and reduction occur at the boron atom (Figure 11b). More precisely, the synergy between the boron atoms located in the meta position with respect to the pyridine nitrogen leads to a lower

adsorption energy of the intermediate on the boron atom (Figure 11c, 11d), and this combination is believed to be responsible for the observed enhanced ORR catalytic activities. Moreover, a theoretical study by Larijani and Khorshidian [171] confirmed the positive synergy of a co-doped B, N carbon material with an increase in the charge density of the boron atom surrounded by a nitrogen atom (see again Figure 9b, 9c).

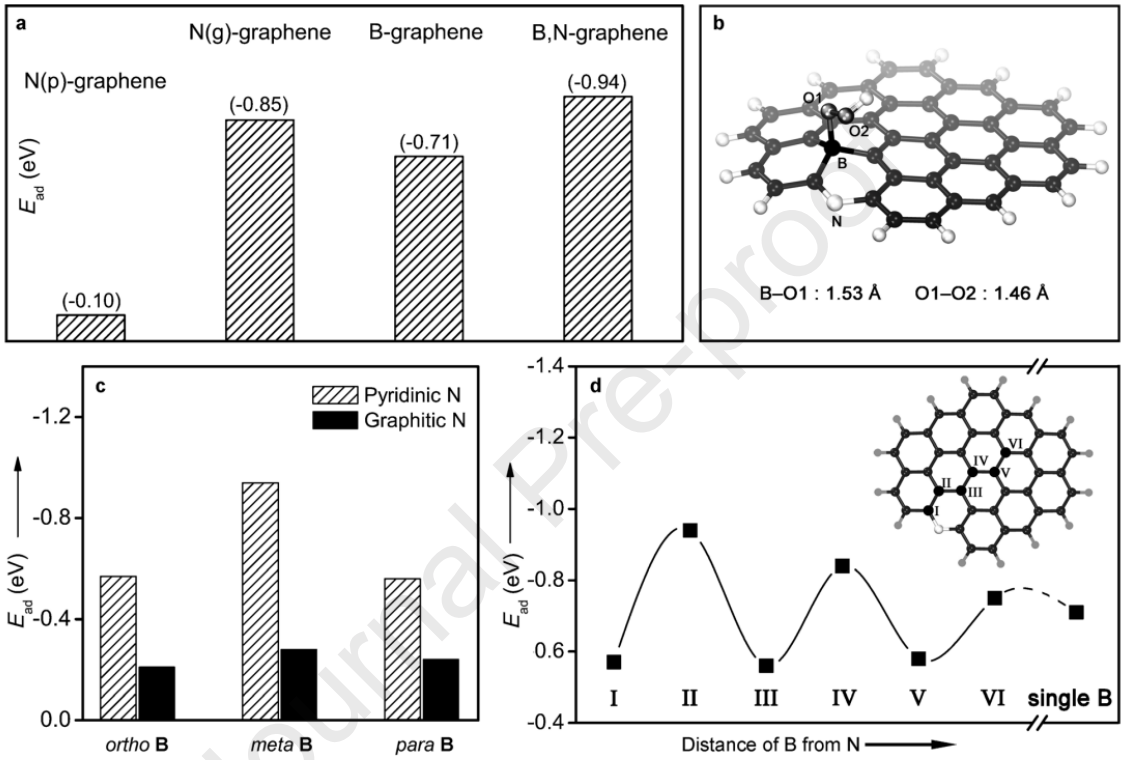

Figure 11. a) Adsorption energies of $HO_2^{\bullet}$ (E_{ad}) on N- and/or B-doped graphene. N(p) and N(g) indicate pyridinic and graphitic N bonding, respectively; b) Optimized configuration of $HO_2^{\bullet}$ adsorbed on B,N-graphene; c) E_{ad} on various B,N-graphene models with pyridinic or graphitic N groups; d) E_{ad} on various B, N-graphene models with B active sites as a function of the distance to a pyridinic N atom (sites I–VI marked in inset). Reprinted from Ref [179], Copyright 2013, with permission from John Wiley and Sons.

4.1.2.4. Nitrogen and fluorine co-doped carbon materials

More recently, nitrogen and fluorine co-doping of carbon materials from biomass precursors has resulted in good catalytic performance for ORR due to the combined effect of these two

heteroatoms [39,180]. In a study of Zhou et al., fluorine doping has been shown to increase the surface wettability of carbonaceous materials by organic electrolytes [181], resulting in improved transport of electrolyte and O_2 to the micropores where the active sites are located. In addition, fluorine is the most electronegative element, which leads to polarization of C-F bonds and induces a delocalization of charge density near these carbon atoms. A DFT study by Peera et al. [182] showed that the presence of pyridinic N and graphitic N atoms in N, F-co-doped carbon nanofibers promotes the formation of semi-ionic C-F bonds and thus increases the catalytic activity in ORR.

4.1.2.5. Tri- and tetra-doped carbon materials

Carbon materials can be doped with more than two different kinds of heteroatoms to further enhance the catalytic properties of the pristine material. Although there are few reports concerning multi-doping [183–185], some works are worth mentioning. Sadeghhassani et al. [183] obtained an N, S, P, B-doped carbon material with an onset potential of 0.90 V vs. RHE and a number of transferred electrons *n* of 4.0 using garlic and graphene as precursors. Although the value of *n* is similar to that of the commercial Pt/C, the E_{ONSET} is still quite far from it. The same observation can be made from the work of Wang et al. [54]. These authors synthesized a tri-doped (N, S and P) carbon material using *E. coli* bacteria and reduced graphene oxide with an E_{ONSET} = 0.88 V vs. RHE, far from that of Pt/C (E_{ONSET} = 0.97 V vs. RHE), and a number of transferred electrons *n* of 3.95, similar to commercial Pt/C. This result can be explained by a possible overestimation of *n* when applying the Koutecky-Levich theory for porous materials [33]. Huang et al. [185] showed through a DFT computational study that the presence of several heteroatoms (N, P and S) in the carbon backbone allows to decrease the energy barrier of the ORR steps, leading to an improved catalytic activity due to the synergistic effect between all these species. Nevertheless, it should be pointed out that specific studies still must be conducted to account for the ORR behavior of each multi-doped carbon material, and that no general rule is found to explain which combination provides the best ORR catalytic performance.

Figure 12 shows E_{ONSET} as a function of the total amount of heteroatoms in catalysts obtained from biomass, and which are reported in the literature [37,40,41,43,48–52,92,111–113,115,116,121,122,124,127–132,136,137,139–156,158,161,166–169,172–175,180,183–186,186–196]. On the one hand, a large dispersion of E_{ONSET} values is observed as a function of the dopant content in the electrocatalyst, which could be explained by the influence of the textural properties and the location of these heteroatoms in the carbon skeleton; this location indeed varies the catalytic activity towards the ORR. The N-doped carbon samples with the best results in terms of E_{ONSET} (i.e., with values closest to those of Pt/C) reported here were obtained from plant biomass precursors, either in the presence of melamine with chemical activation during the synthesis process, or in the presence of an NH_3 stream during the pyrolysis of the samples, or from N-rich animal biomass precursors (silk cocoons). It is interesting to note that all the final products present relatively large specific surface areas (for most of them, A_{BET} > 1000 $m^2\ g^{-1}$) favoring the contact of the O_2-saturated electrolyte with the material and thus facilitating the interaction between oxygen and active sites with important proportions of pyridinic N and graphitic N (the proportion of both types of N representing at least 58 % of the total N introduced in the carbonaceous materials). On the other hand, it is imperative to adapt or to adjust the amount of dopant that one wishes to introduce into the material to have an effective electrocatalyst for the ORR. While a minimum of active sites is required to be able to reduce the dioxygen molecules (as seen at the lowest doping level), the addition of an excess of dopant (at about 8 at.%) negatively affects the catalytic activity, as evidenced by the drop in the onset potential; this drop is a consequence of a decrease in the electrical conductivity or porosity of the carbonaceous material [138,197]. Therefore, it is important to control the doping level during the development of an electrocatalyst, and some of the metal-free electrocatalysts shown in Figure 12 have an onset potential equal to or close to that of commercial Pt/C-based electrocatalysts reported in literature.

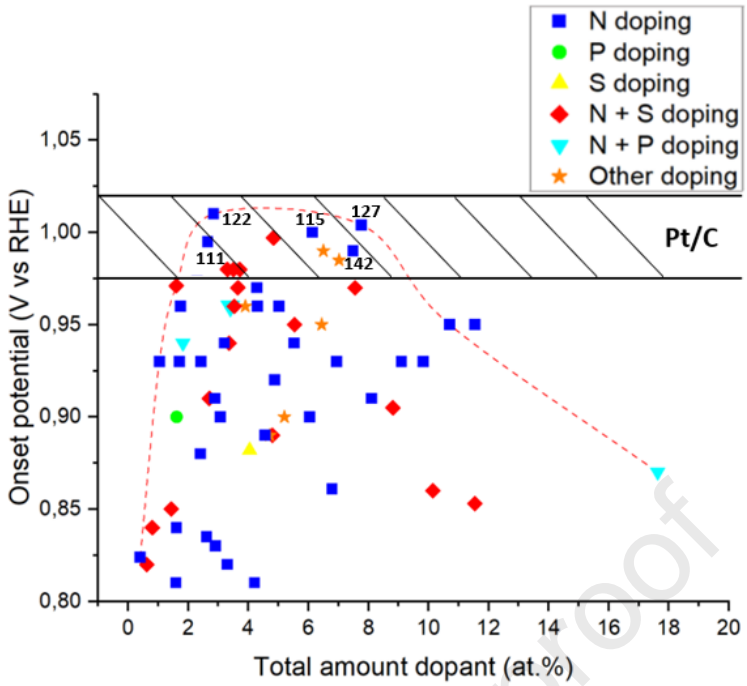

References	Carbon precursors	N-doping agent	Activation	E_{ONSET}	A_{BET}	N-content	N-pyridinic	N-graphitic
142	Silk cocoons	X	$ZnCl_2$	0.99	1274	7.49	0.91	4.04
111	*Scindapsus*	NH_3 flux	X	0.995	1599	2.65	1.07	0.58
127	Water lettuces	NH_3 flux	X	1.00	823	7.76	2.63	1.99
115	Papaya skins	Melamine	$KHCO_3$	1.00	1671	6.13	2.38	1.65
122	Coconut palm leaves	Melamine	$KHCO_3$+KOH	1.01	1419	2.84	0.64	1.01

Figure 12. Onset potential measured in alkaline medium as a function of total amount of dopant in biomass-derived, heteroatom-doped carbon catalysts from the literature [37,40,41,43,48–52,92,111–113,115,116,121,122,124,127–132,136,137,139–156,158,161,166–169,172–175,180,183–186,186–196].

The electrocatalysts are separated into several families in the figure: mono-doping with N, P or S, co-doping with N + S or N + P, and all others: co-doping with other heteroatoms or multi-doping. The N-doped carbon materials obtained with the closest E_{ONSET} to that of Pt/C have been reported in the table along with the biomass precursor, the nitrogen external source and the activation used during the synthesis procedure (if any), the BET area, and the total nitrogen, pyridinic N and graphitic N contents. Different types of biomass-derived multi-doped carbon electrocatalysts have been reported in Table 2 along with the results obtained in ORR.

901 **Table 2.** Metal-free and multi-doped carbon electrocatalysts for ORR. Electrochemical data
902 were obtained in 0.1 M KOH electrolyte.

Biomass source	Other sources	Synthesis method	Doping atoms (at.%)	Specific surface area ($m^2\ g^{-1}$)	Total pore volume ($cm^3\ g^{-1}$)	E_{ONSET} (V vs. RHE)	$E_{1/2}$ (V vs. RHE)	j_l (mA cm^{-2}) at 1600 rpm	Number of transferred electrons *n*	Ref.
Sweet potato vine	--	Pyrolysis	N: 1.2 S: 0.23	885	0.52	0.85	0.65	--	~4	[166]
Honey-suckles	--	Pyrolysis	N: 1.95 S: 0.75	803	0.49	0.91	0.77	--	3.6	[167]
Sheep horns	Graphene oxide	Ball milling, pyrolysis	N: 3.14 S: 0.22	320	--	--	0.78	5.41 at 0.1 V vs. RHE	3.52-3.83	[168]
Rapeseed meal	$ZnCl_2$	Carbonization, activation	N: 3.0 S: 0.5	1564	0.8	0.98	0.76	--	3.5-3.9	[169]
Bagasse lignin	Melamine Urea	Immersion, pyrolysis	N: 4.18 S: 0.65	1208	1.4	1.00	0.86	4.67 at 0.1 V vs. RHE	~4	[172]
Poplar catkins	--	Immersion, pyrolysis, activation under CO_2	N: 0.27 S: 0.35	604	0.35	0.82	0.76	4.6 at 0.2 V vs. RHE	3.9-4.0	[173]
Mulberry leaves	KOH Thiourea	Activation, freeze-drying, pyrolysis	N: 8.17 S: 1.97	1689	1.01	0.86	--	--	3.7-3.9	[116]
Silk cocoon (*Astridia velutina*)	KOH Thiourea	Activation, pyrolysis	N: 9.75 S: 1.79	377	--	0.85	0.72	4.5 at 0 V vs. RHE	~4	[174]
Allium cepa	Thiourea KOH	Immersion, activation, pyrolysis	N: 5.32 S: 2.23	1859	--	0.97	0.82	5.63 at 0.2 V vs. RHE	3.95	[175]
Keratin	KOH NH_3	Carbonization, activation, pyrolysis	N: 1.5 S: 0.1	1799	1.01	0.97	0.84	--	3.8	[186]
Alkaline lignin	Urea	Pyrolysis	N: 2.98 S: 0.67	1209	0.74	0.97	0.83	--	3.8	[188]
Lotus seedpods	Melamine Phytic acid	Carbonization, pyrolysis	N: 15.95 P: 1.68	270	--	0.87	--	--	3.6-4.0	[191]

E. coli	Graphene oxide	Culture bacteria, impregnation, lyophilization, pyrolysis	N: 2.42 P: 1.25 S: 0.42	288	--	0.88	--	--	3.95	[54]
Lignin	Urea Melamine $ZnCl_2$ $NaCl_2$	Immersion, freeze-drying, pyrolysis	N: 3.35 S: 0.8 Cl: 0.59	1290	2.81	0.89	0.79	6.93 at 0.1 V vs. RHE	3.93	[184]
Spinach leaves	$ZnCl_2$	Activation, pyrolysis	N: 5.43 P: 0.71 S: 0.30	1145	--	0.95	0.82	5.19 at 0.5 V vs. RHE	3.81	[185]

4.2.Non-precious metal-doped carbon materials (NPMCs)

Besides metal-free carbon-based electrocatalysts, non-precious metal-containing carbon-based electrocatalysts are a promising alternative to replace platinum-based electrodes in the cathode electrode of fuel cells. Non-precious metal atoms are considered to be highly effective active sites for ORR. However, the stability of these species needs to be improved. In this sense, metal-N bonds are highly recommendable to create robust and efficient ORR electrocatalysts based on non-precious metals, since nitrogen species are known as excellent anchoring points to provide stability to metal active sites [91,198]. In this section, the influence of the presence of one or more metals in the heteroatom-rich carbon backbone on the ORR catalytic properties of these materials is discussed. Table 3 provides a concise summary of some non-precious metal-doped carbon catalysts derived from biomass along with their ORR properties in alkaline media.

919 **Table 3.** Non-precious metal-doped carbon electrocatalysts for ORR. Electrochemical data

920 were obtained in 0.1 M KOH electrolyte.

Biomass source	Other sources	Synthesis method	Doping atoms (at.%)	Specific surface area ($m^2\ g^{-1}$)	Total pore volume ($cm^3\ g^{-1}$)	E_{ONSET} (V vs. RHE)	$E_{1/2}$ (V vs. RHE)	j_l (mA cm^{-2}) at 1600 rpm	Number of transferred electrons *n*	Ref.
Cellulose	KOH $FeCl_3$ NH_3	HTC, activation, microwave radiation, oxidation, microwave ammoxidation	N: 1.5 wt.% (EA) Fe: --	1261	1.03	0.91	0.81	--	3.9	[99]
Sugarcane	KOH $FeCl_3$ $CoCl_2$ NH_3	HTC, impregnation, activation, microwave ammoxidation	N : 1.5 Fe : --	857	0.66	0.91	0.81	--	3.8-3.9	[100]
Wood briquettes	$FeCl_3$ H_3PO_4	Impregnation, pyrolysis	N: 3.84 P: 0.57 Fe: 0.53	1608	0.73	1.10	0.89	--	3.88	[199]
Brewer's yeast powder	$FeCl_3$ Liquid NH_3 NH_3	HTC, pyrolysis	N: 3.9 P: 0.46 Fe: 0.8	290	--	0.99	0.86	5.64 at 0.2 V vs. RHE	3.86-3.93	[74]
Douglas fir sawdust	Melamine $Fe(NO_3)_3$ solution	HTC, pyrolysis	N: 2.9 Fe: <0.6	765	--	0.91	0.78	5.86 at 0.5 V vs. RHE	3.4-3.8	[200]
Glucose	Melamine $FeSO_4•7H_2O$	Pyrolysis	N: 5.21 Fe: 0.48	393	0.99	0.87	--	5.21 at 0.5 V vs. RHE	3.77	[201]
Wheat flour	$Fe(NO_3)_3•9H_2O$	Silica templating, pyrolysis, immersion, pyrolysis	N: 3.78 Fe: 0.25	365	0.55	0.98	0.86	--	3.96	[202]
Soybean straw	Melamine Magnesium oxide	Pyrolysis	N: 5.56 Fe: 0.4	521	2.2	0.99	0.85	--	3.94	[42]
Starch	Ferric nitrate Graphene oxide $FeCl_3$ KSCN	HTC, impregnation, pyrolysis	N: 2.22 S: 0.56 Fe: 0.31	750	--	0.95	0.83	--	3.96	[203]
Shrimp shells	Phosphoric acid	HTC, pyrolysis	N: 2.51 P: 1.42 Fe: 0.32	857	0.55	0.96	0.82	4.47 at 0.2 V vs. RHE	3.78	[204]

Agaricus bisporus	$(NH_4)_3PO_4$ $ZnCl_2$ $FeCl_3•6H_2O$	HTC, activation, pyrolysis	N: 2.36 P: 0.46 Fe: 0.76	1646	0.901	0.97	0.82	4.47 at 0.3 V vs. RHE	3.91	[53]
Shewanella oneidensis MR-1	--	Culture and fixation bacteria, pyrolysis	N: 2.26 S: 0.1 P: 0.46 Fe: 0.18	142	--	0.98	0.83	--	3.9	[56]
Vitamin B_2	NaCl $Co(OAc)_2•4H_2O$	Lyophilization, pyrolysis	N: 4.6 Co: 0.6	513	0.32	0.97	0.86	--	3.98	[205]
Root nodules	$ZnCl_2$	Carbonization, activation, pyrolysis	N: 1.45 S: 0.36 Mo: 0.05 Fe: 0.106 wt.%	1838	1.19	0.97	0.87	5.23 at 0.2 V vs. RHE	3.63-3.99	[206]
Pig blood	$Zn(NO_3)_2•6H_2O$ NH_3	Purification of blood, HTC, pyrolysis	N: 6 wt.% Fe: 1.3 wt.% Zn: 0.2 wt.%	1260	2.94	1.00	0.87	--	~4	[207]

Non-precious metal-based active sites can be found in multiple forms, such as nanoparticles, clusters or even single-atom arrangement. Single-atom catalysts (SACs) are noteworthy because full atomic exposure is achieved if the metal is atomically dispersed in the carbon material, exposing the greatest number of the active sites [208,209]. In 1964, Jasinski [210] first showed that a transition metal in a porphyrin (cobalt phthalocyanine in the study) could exhibit ORR catalytic activity in alkaline media through the formation of metal complexes in which the central metal atoms binds to four nitrogen atoms. Nevertheless, these compounds have relatively poor stability in acidic media where the metals are leached by the electrolyte at low pH, leading to a degradation of the catalytic properties of the material. In order to increase the catalytic stability of these single atoms, it is recommended to introduce the metal atoms into a well-structured and stable support, especially N-doped carbon materials. Heat treatment of metal porphyrin can produce metal and N-co-doped carbon materials with improved ORR activity [91]. Since the discovery of the high activity of SACs, the development of carbon-based

electrocatalysts that contain nitrogen and metals (denoted M-N-C) has become a challenging goal of the scientific community. These catalysts can be obtained by using metal-containing macrocycles instead, as was the case for Jasinski [210], or from less expensive compounds that are intrinsically metal-rich in nature [211], such as biomass containing metal impurities.

Iron is the most widely used and the cheapest transition metal (Figure 13) for the production of non-precious metal carbon catalysts for ORR [212]. It has been repeatedly observed that the introduction of iron into the carbon backbone promotes graphitization of the carbon material upon pyrolysis at high temperature, which allows for an increase in the electrical conductivity of the sample and facilitates electron transport [213–216]. Nevertheless, the iron doping level of the carbon-based catalyst does not correlate linearly with the catalytic activity in ORR. Therefore, it is important to select not only the right doping level but also the type of Fe species to have optimal catalytic activity in ORR. Indeed, Kuo et al. [99] developed an N- and Fe-doped catalyst by hydrothermal synthesis of cellulose at 180 °C for 16 hours, and then the resulting solid was mixed with $FeCl_3$ in different proportions, followed by two microwave irradiations (the first under inert gas and the second under NH_3 flow). They observed a similar onset potential and half-wave potential for 1 wt.% and 5 wt.% iron doping in the N-doped carbon material (E_{ONSET} = 0.91 V vs. RHE; $E_{1/2}$ = 0.81 V vs. RHE), but a lower limiting current density was observed in the second case (3.2 mA cm^{-2} and 1.4 mA cm^{-2}, respectively).

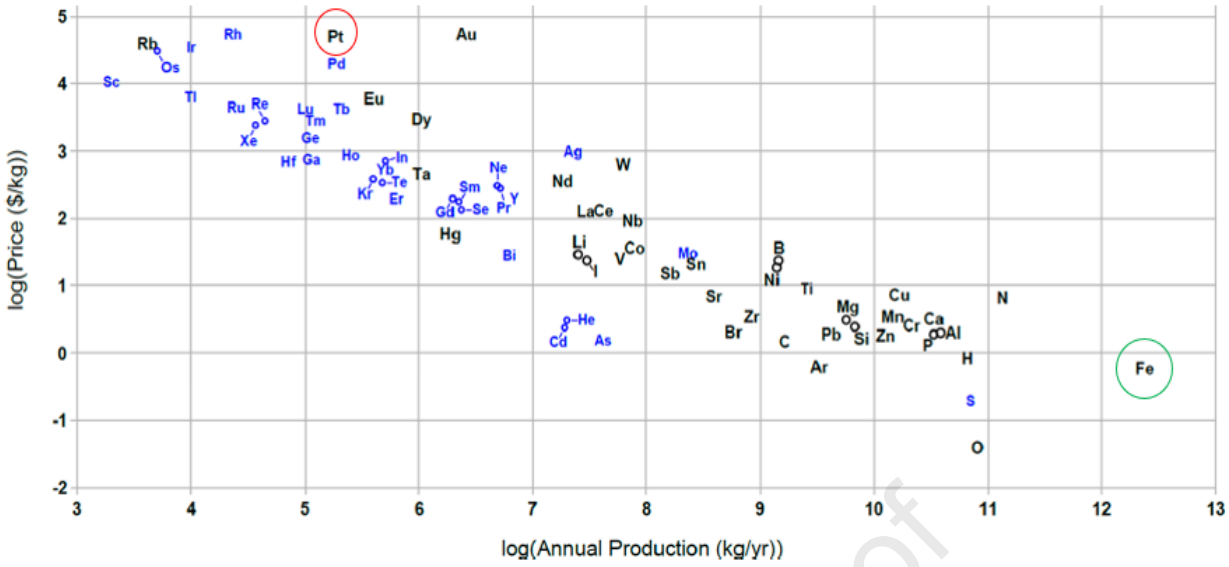

954

955 **Figure 13.** Price of different elements as a function of their annual production (adapted with
956 permission form Ref. [212]. Copyright 2016 American Chemical Society).

957 Excessive iron doping in a carbon catalyst doped with heteroatoms does not always lead to
958 better performance in terms of onset potential and half-wave potential, since Fe nanoparticles
959 can: (i) block the porosity where most of the active sites are located; or (ii) lead to agglomeration
960 that decreases the ORR activity [198,199,217]. Other authors [199] have shown that increasing
961 the level of Fe doping in a N, P-co-doped carbon catalyst improves the onset potential and half-
962 wave potential to an optimized value of 1.86 wt.%. The authors attributed this optimum to a
963 homogeneous dispersion of the iron in the carbon lattice. Above 1.86 wt.% Fe, a slight decrease
964 in electrocatalytic activity is observed, attributed to agglomeration of iron particles and thus to
965 a decrease in the number of active sites. The same trend was also observed by Wang et al. [74]
966 for their N, P and Fe-tri-doped carbon catalyst prepared by using brewer's yeast powder,
967 ammonium hydroxide and iron chloride as precursors.

968 Nevertheless, as with nitrogen, it is not the total iron content that is critical to the ORR
969 catalytic activity but the type of iron species. The work of Kramm et al. [218] highlighted the
970 possible presence of several iron species in Fe-N-C type catalysts using ^{57}Fe Mössbauer
971 spectroscopy, including FeN_4 sites with iron ions in a different spin state, Fe_xN sites (with $x \leq$

2.1), and iron nitrides with a stoichiometry between those of Fe_xN and FeN_4 sites. This study showed that FeN_4 species with ferrous ions in a high spin state and a low spin state present high catalytic activity in ORR with improved stability in acidic media. The two active sites that are predominantly present in Fe-N-C type electrocatalysts are the Fe-N_4 "in-plane" sites located in the middle of the planes, and the Fe-N_{2+2} "edge" sites present in the micropores (Figure 14a) [219]. For example, by ^{57}Fe Mössbauer spectroscopy, Pérez-Rodriguez et al. [220] detected in their carbonaceous material FeN_4 groups with ferrous ions in a low spin state that are associated with the good performance observed in ORR in alkaline medium ($E_{1/2}$ = 0.78 V vs. RHE). In general, O_2 molecules are directly chemisorbed onto iron (the center of the FeN_4 active site) in two possible ways: end-on configuration (Figure 14b) or side-on configuration (Figure 14c) before being reduced into hydroxide peroxide or/and water [221].

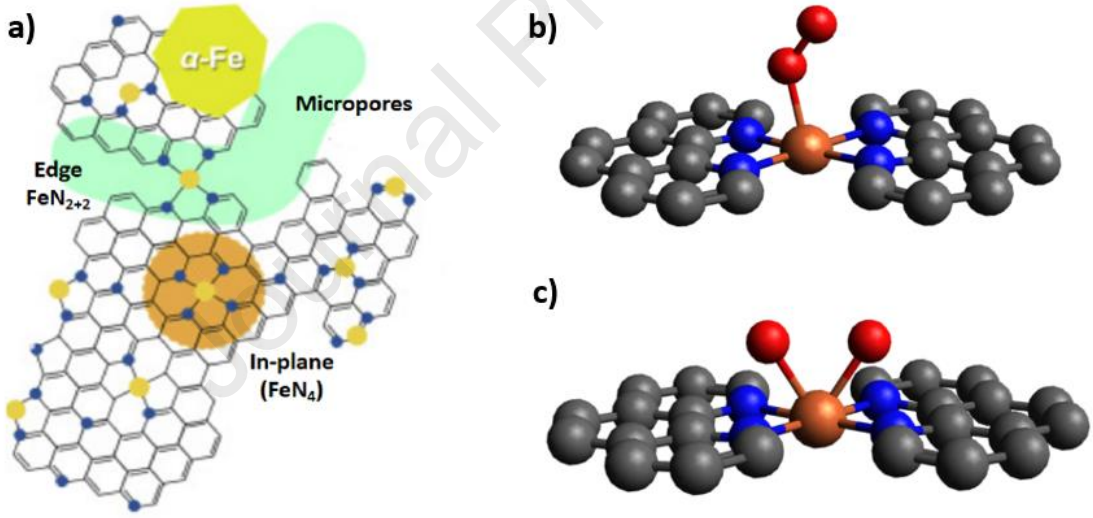

Figure 14. a) Schematic representation of the different sites present in a Fe-N-C material (adapted from Ref. [219], Copyright 2020, with permission from Elsevier). Optimized geometries of O_2 adsorbed on FeN_4 clusters: b) end-on and c) side-on configurations (adapted from Ref. [221], Copyright 2013, with permission from Royal Society of Chemistry).

In addition to nitrogen, other heteroatoms such as phosphorus can be introduced into the carbon material to serve as metal anchors and thus increase the synergies between the different

functionalities present in the material by increasing the number and type of active sites. Qin et al. [222] found Fe_2P species in biomass-derived carbon materials after hydrothermal synthesis using potassium ferricyanide and egg yolks, followed by pyrolysis at 1000 °C for 2h under NH_3 flow. The authors attributed the high catalytic performance towards the ORR to the presence of these iron-phosphorus species. Similarly, Li et al. [204] showed the importance of incorporating phosphorus into the N, P and Fe tri-doped carbon material (P/Fe/N-SS) derived from shrimp shells, H_3PO_4 and $FeCl_3$ as sources of nitrogen, phosphorus, and iron respectively. The authors performed the same synthesis without the addition of phosphorus (Fe/N-SS) and observed a decrease in E_{ONSET} and $E_{1/2}$ by 5 mV and 4 mV, respectively. The authors attributed the observed differences in catalytic activity in ORR to the presence of FeP species detected by XPS in the P/Fe/N-SS tri-doped sample. Other works have also proved the catalytic activity of iron-phosphorus species in the ORR [199,223]. As in the case of metal-free catalysts, multi-doping with heteroatoms can be achieved to create synergistic effects. A tetra-doped (N, S, P and Fe) porous carbon material was obtained by Guo et al. [56] following the decomposition of *Shewanella oneidensis* MR-1 bacteria by direct pyrolysis. The authors obtained excellent electrochemical performance (E_{ONSET} = 0.98 V vs. RHE; $E_{1/2}$ = 0.83 V vs. RHE), comparable to Pt/C. According to the characterization, this was attributed to a synergy between the different heteroatoms along with the porous structure of their material.

Another relevant metallic arrangement that has not been mentioned previously is the core-shell encapsulation of metal nanoparticles by graphene-like carbon layers. Although not in direct contact with the electrolyte and dioxygen molecules, it has been shown that metal entities encapsulated in graphene sheets can improve ORR performances [213]. In the work of Hu et al. [224], encapsulation of iron carbide Fe_3C nanoparticles in N-doped graphitic layers showed improved catalytic properties in ORR and stability in both acidic and alkaline media, a rare fact attributed to the synergy between the protective graphenic layers and the carbides nanoparticles.

These nanoparticles allow an activity of the graphenic layers of the shell surrounding the core particle, in terms of induced changes in the electron density of the carbon atoms of the graphene-like layers that promote the ORR. This observation was also made by Wang et al. [225] where the authors attributed the ORR performance of N- and Fe-doped carbon materials to the presence of these Fe_3C nanoparticles. Other researchers [35,200,201] have also observed an enhancement of the catalytic activity of their material by these core-shell nanoparticles in carbon materials. The chemistry behind this behavior was explained by DFT calculations [226]. A metallic iron nanoparticle encapsulated under the N-doped carbon layers provides a large number of electrons to the carbon shells, which are then used in the active sites of the carbon layers to chemisorb and reduce dioxygen molecules. This core-shell conformation is not only effective when iron carbides are used, but also works with Fe_3O_4 [42,202,227]. In addition, other metals such as Co [227], Ni [227], etc. can also produces core-shell metal configurations in which improved catalytic activity is observed.

Other metals for ORR electrocatalysis such as Co [115,205,217,228–230], Mo [231], and Mn [232] have emerged as excellent active sites in biomass-derived carbon materials to further improve the catalytic activity for oxygen reduction. These metals exhibited excellent catalytic activities, similar or better than those of Fe-based electrocatalysts, but it should be noted that the cost of these metal is higher than that of Fe. Liu et al. [229] produced a Co, N-co-doped carbon material from corn stover with an $E_{1/2}$ of 0.743 V vs. RHE in alkaline medium, close to that of Pt/C 20 wt.% ($E_{1/2}$ = 0.793 V vs. RHE), mainly attributed to the proportion of graphitic N, pyridinic N, and Co embedded in the carbon matrix. DFT calculations showed that single Co atoms bonded to two, three or four nitrogen atoms (CoN_2 [233], CoN_3 [234], or CoN_4 [235]) provide excellent ORR activity ($E_{ONSET} \leq$ 0.95 V vs. RHE in alkaline medium), and that the most important parameter on ORR activity is the valence electron occupancy of Co *d*-orbitals. Nevertheless, Co nanoparticles were also found to be effective in the reduction of dioxygen

molecules [236]. As mentioned above, highly efficient biomass-derived electrocatalysts can also be based on Mo, Mn, Ni, Cu, etc. A more in-depth explanation of the effect of each metal and the origin of catalytic activity in ORR performance can be found in the literature [237–241].

Another promising alternative is the use of two or more metals to induce synergistic effects that could enhance the ORR performance, similar to the multi-doping of carbon materials. Kuo et al. [100] obtained two Fe-Co, N-doped carbon material from sugarcane and palm kernel shell by hydrothermal synthesis and microwave ammoxidation. They obtained for both kinds of materials an E_{ONSET} of about 0.90 V vs. RHE and $E_{1/2}$ of 0.80 V vs. RHE in alkaline medium, and their performance was attributed to the FeCo/N species embedded in the porous carbon material. On the other hand, Hao et al. [206] obtained a carbon material from plant root nodules, intrinsically doped with N, S, Fe and Mo since these heteroatoms were initially present in the starting biomass precursor. The metals in the roots were indeed taken up from the soil by the plant for growth and contributed to the catalytic performances in ORR although they were only present in trace amounts (0.05 wt.% Mo and 0.1 wt.% Fe, measured by ICP).

5. Conclusion and perspectives

The valorization of biomass as carbon-based catalysts materials has been reported as a promising alternative to platinum based-electrocatalysts for the oxygen reduction reaction (ORR), mainly in alkaline media where overpotentials and kinetics are favorable. In fact, biomass resources are considered the main green source of carbon precursors with a wide variety of properties and applications. All carbon materials have intrinsic characteristics that affect ORR catalytic activity. Textural properties appear to be of paramount importance to ensure the accessibility of the dioxygen molecules from the electrolyte to the active sites, which seem to be located in the microporosity of carbon materials. Nevertheless, other parameters such as defects have proven to be of great interest by acting as active sites where oxygen

molecules are chemisorbed and reduced. Therefore, the design of an advanced electrocatalyst requires the creation of well-developed porosity in carbon materials, whether the active sites are based on metals or heteroatoms. In this review, the ORR performance in alkaline medium of recent bio-based carbon electrocatalysts has been reported and compared to understand better the influence of different physicochemical properties on the ORR.

Biomass-derived carbon materials are inherently rich in heteroatoms, which are a different form of defects in the carbon structure. These heteroatoms cause significant changes in the electron density distribution in the carbon matrix, localizing charges in the carbon atoms adjacent to the heteroatoms. This localized charge density can act as an active site, where oxygen molecules can be easily chemisorbed and reduced, resulting in improved catalytic performance compared to the homogenous charge distribution of undoped carbon materials. Among all heteroatoms, nitrogen-based functionalities have been reported to be the most influential species in ORR, both theoretically and experimentally. In particular, pyridinic N and graphitic N are proposed as the most active functionalities for the ORR of biomass-derived carbons. The introduction of other heteroatoms, such as sulfur, phosphorus or boron into carbon materials have also shown positive effects, but the origin of the catalytic activity is still under debate. The literature proposes two main hypotheses: (i) the heteroatoms are intrinsic active sites; or (ii) the defects produced by the introduction of these heteroatoms are the ones that truly behave as active sites towards the ORR. The identification of active sites and the origin of catalytic activity in heteroatom-doped carbon materials have become one of the most challenging goals in materials science.

Electrocatalysts based on non-precious metals have also been extensively studied in the literature, as different metals have been shown to catalyze the ORR as efficiently as platinum-based electrodes, especially in alkaline media. This effect is particularly noticeable in carbonaceous materials containing both nitrogen and metal. The role of the N species is to act

as anchor points where the metal species are attached. At the same time, the metal atoms are responsible for the reduction of dioxygen molecules. The combination of metal atoms and N species often leads to highly efficient ORR performance with improved stability. The most interesting metal-containing electrocatalysts are based on Fe and Co, which exhibit excellent ORR performances at a competitive cost. Another important discussion about metal-containing electrocatalysts derived from biomass concerns the origin of the catalytic activity. Metals can be found in multiple configurations (surface nanoparticles, clusters and single atoms, and encapsulated nanoparticles), and all are proposed to be responsible for high catalytic behaviors. Future research on the precise role of metal configuration and species as well as different co-doping materials should be considered for the preparation of excellent biomass-derived materials for the ORR.

Most researchers are currently focusing their work on evaluating the ORR behavior of carbon materials in alkaline media. Yet, it is widely known that the most optimized fuel cell stations are based on proton-exchange membranes, which means that the cathode electrode is immersed in an acidic medium. The catalytic activity of most carbon-based electrocatalysts in an alkaline medium is significantly higher than that obtained in an acidic environment. Pending significant improvement of anion-exchange membranes, future research should therefore also focus on the development of stable and efficient electrocatalysts in acidic media, including finding strategies to minimize the problems of carbon corrosion and leaching of the non-precious metals involved.

Biomass-derived nanomaterials have attracted increasing interest and rapid development in the future is possible, especially for energy conversion applications, given the renewable, very abundant and inexpensive aspects of biomass, which can compete with conventional chemical precursors often derived from the oil industry. Moreover, these bio-based porous carbon materials can be used in other applications such as supercapacitors, CO_2 capture or other

catalytic reactions. Therefore, the search for synthesis protocols using "green precursors" such as biomass should be privileged in order to meet the energy needs of society in a sustainable way.

Acknowledgements

This study was partly supported by the French PIA project “Lorraine Université d’Excellence”, reference ANR-15-IDEX-04-LUE and the TALiSMAN project funded by ERDF (2019-000214). JQB thanks the Ministerio de Universidades, the European Union and the University of Alicante for the financial support of his Margarita Salas fellowship (MARSALAS21-21).

References

[1] L’Accord de Paris | CCNUCC, (2015). https://unfccc.int/fr/processus-et-reunions/l-accord-de-paris/l-accord-de-paris (accessed March 9, 2022).
[2] J. Zhang, ed., PEM Fuel Cell Electrocatalysts and Catalyst Layers, Springer London, London, 2008. https://doi.org/10.1007/978-1-84800-936-3.
[3] Z.-L. Wang, D. Xu, J.-J. Xu, X.-B. Zhang, Oxygen electrocatalysts in metal–air batteries: from aqueous to nonaqueous electrolytes, Chem Soc Rev. 43 (2014) 7746–7786. https://doi.org/10.1039/C3CS60248F.
[4] F. Cheng, J. Chen, Metal–air batteries: from oxygen reduction electrochemistry to cathode catalysts, Chem. Soc. Rev. 41 (2012) 2172. https://doi.org/10.1039/c1cs15228a.
[5] M. Borghei, J. Lehtonen, L. Liu, O.J. Rojas, Advanced Biomass-Derived Electrocatalysts for the Oxygen Reduction Reaction, Adv. Mater. 30 (2018) 1703691. https://doi.org/10.1002/adma.201703691.
[6] X. Huang, T. Shen, S. Sun, Y. Hou, Synergistic Modulation of Carbon-Based, Precious-Metal-Free Electrocatalysts for Oxygen Reduction Reaction, ACS Appl. Mater. Interfaces. 13 (2021) 6989–7003. https://doi.org/10.1021/acsami.0c19922.
[7] T. Shen, X. Huang, S. Xi, W. Li, S. Sun, Y. Hou, The ORR electron transfer kinetics control via Co-N and graphitic N sites in cobalt single atom catalysts in alkaline and acidic media, J. Energy Chem. 68 (2022) 184–194. https://doi.org/10.1016/j.jechem.2021.10.027.
[8] M.K. Debe, Electrocatalyst approaches and challenges for automotive fuel cells, Nature. 486 (2012) 43–51. https://doi.org/10.1038/nature11115.
[9] S. Shen, R. Zhou, Y. Li, B. Liu, G. Pan, Q. Liu, et al., Bacterium, Fungus, and Virus Microorganisms for Energy Storage and Conversion, Small Methods. 3 (2019) 1900596. https://doi.org/10.1002/smtd.201900596.
[10] Z. Wang, D. Shen, C. Wu, S. Gu, State-of-the-art on the production and application of carbon nanomaterials from biomass, Green Chem. 20 (2018) 5031–5057. https://doi.org/10.1039/C8GC01748D.
[11] N. Tripathi, C.D. Hills, R.S. Singh, C.J. Atkinson, Biomass waste utilisation in low-carbon products: harnessing a major potential resource, Npj Clim. Atmospheric Sci. 2 (2019) 35. https://doi.org/10.1038/s41612-019-0093-5.

[12] K.A. Motghare, A.P. Rathod, K.L. Wasewar, N.K. Labhsetwar, Comparative study of different waste biomass for energy application, Biowaste Fuel. 47 (2016) 40–45. https://doi.org/10.1016/j.wasman.2015.07.032.
[13] M.V. Rodionova, R.S. Poudyal, I. Tiwari, R.A. Voloshin, S.K. Zharmukhamedov, H.G. Nam, et al., Biofuel production: Challenges and opportunities, Int. J. Hydrog. Energy. 42 (2017) 8450–8461. https://doi.org/10.1016/j.ijhydene.2016.11.125.
[14] Y. Wang, Y.-J. Hu, X. Hao, P. Peng, J.-Y. Shi, F. Peng, et al., Hydrothermal synthesis and applications of advanced carbonaceous materials from biomass: a review, Adv. Compos. Hybrid Mater. 3 (2020) 267–284. https://doi.org/10.1007/s42114-020-00158-0.
[15] P. Kaur, G. Verma, S.S. Sekhon, Biomass derived hierarchical porous carbon materials as oxygen reduction reaction electrocatalysts in fuel cells, Prog. Mater. Sci. 102 (2019) 1–71. https://doi.org/10.1016/j.pmatsci.2018.12.002.
[16] Y. Wang, M. Zhang, X. Shen, H. Wang, H. Wang, K. Xia, et al., Biomass-Derived Carbon Materials: Controllable Preparation and Versatile Applications, Small. 17 (2021) 2008079. https://doi.org/10.1002/smll.202008079.
[17] S. De, A.M. Balu, J.C. van der Waal, R. Luque, Biomass-Derived Porous Carbon Materials: Synthesis and Catalytic Applications, ChemCatChem. 7 (2015) 1608–1629. https://doi.org/10.1002/cctc.201500081.
[18] C. Ouyang, X. Wang, Recent progress in pyrolyzed carbon materials as electrocatalysts for the oxygen reduction reaction, Inorg. Chem. Front. 7 (2020) 28–36. https://doi.org/10.1039/C9QI00962K.
[19] L. Du, G. Zhang, X. Liu, A. Hassanpour, M. Dubois, A.C. Tavares, et al., Biomass-derived nonprecious metal catalysts for oxygen reduction reaction: The demand-oriented engineering of active sites and structures, Carbon Energy. 2 (2020) 561–581. https://doi.org/10.1002/cey2.73.
[20] B. Szczęśniak, J. Phuriragpitikhon, J. Choma, M. Jaroniec, Recent advances in the development and applications of biomass-derived carbons with uniform porosity, J. Mater. Chem. A. 8 (2020) 18464–18491. https://doi.org/10.1039/D0TA05094F.
[21] H.S. Wroblowa, Yen-Chi-Pan, G. Razumney, Electroreduction of oxygen, J. Electroanal. Chem. Interfacial Electrochem. 69 (1976) 195–201. https://doi.org/10.1016/S0022-0728(76)80250-1.
[22] R. Coulon, Modélisation de la dégradation chimique de membranes dans les piles à combustibles à membrane électrolyte polymère, Université de Grenoble, 2012. https://tel.archives-ouvertes.fr/tel-00767412.
[23] Z.-F. Huang, J. Wang, Y. Peng, C.-Y. Jung, A. Fisher, X. Wang, Design of Efficient Bifunctional Oxygen Reduction/Evolution Electrocatalyst: Recent Advances and Perspectives, Adv. Energy Mater. 7 (2017) 1700544. https://doi.org/10.1002/aenm.201700544.
[24] J. Wang, C.-X. Zhao, J.-N. Liu, D. Ren, B.-Q. Li, J.-Q. Huang, et al., Quantitative kinetic analysis on oxygen reduction reaction: A perspective, Nano Mater. Sci. 3 (2021) 313–318. https://doi.org/10.1016/j.nanoms.2021.03.006.
[25] J. Zhang, Q. Li, C. Zhang, L. Mai, M. Pan, S. Mu, A N-self-doped carbon catalyst derived from pig blood for oxygen reduction with high activity and stability, Electrochimica Acta. 160 (2015) 139–144. https://doi.org/10.1016/j.electacta.2015.01.200.
[26] J. Zhang, Q. Li, H. Wu, C. Zhang, K. Cheng, H. Zhou, et al., Nitrogen-self-doped carbon with a porous graphene-like structure as a highly efficient catalyst for oxygen reduction, J. Mater. Chem. A. 3 (2015) 10851–10857. https://doi.org/10.1039/C5TA00547G.
[27] G. Zhang, Q. Wei, X. Yang, A.C. Tavares, S. Sun, RRDE experiments on noble-metal and noble-metal-free catalysts: Impact of loading on the activity and selectivity of oxygen reduction reaction in alkaline solution, Appl. Catal. B Environ. 206 (2017) 115–126. https://doi.org/10.1016/j.apcatb.2017.01.001.
[28] G. Wu, K.L. More, C.M. Johnston, P. Zelenay, High-Performance Electrocatalysts for Oxygen Reduction Derived from Polyaniline, Iron, and Cobalt, Science. 332 (2011) 443–447. https://doi.org/10.1126/science.1200832.

[29] G. Lemes, D. Sebastián, E. Pastor, M.J. Lázaro, N-doped graphene catalysts with high nitrogen concentration for the oxygen reduction reaction, J. Power Sources. 438 (2019) 227036. https://doi.org/10.1016/j.jpowsour.2019.227036.
[30] S. Treimer, A. Tang, D.C. Johnson, A Consideration of the Application of Koutecký-Levich Plots in the Diagnoses of Charge-Transfer Mechanisms at Rotated Disk Electrodes, Electroanalysis. 14 (2002) 165. https://doi.org/10.1002/1521-4109(200202)14:3<165::AID-ELAN165>3.0.CO;2-6.
[31] L. Bouleau, S. Pérez-Rodríguez, J. Quílez-Bermejo, M.T. Izquierdo, F. Xu, V. Fierro, et al., Best practices for ORR performance evaluation of metal-free porous carbon electrocatalysts, Carbon. 189 (2022) 349–361. https://doi.org/10.1016/j.carbon.2021.12.078.
[32] Z. Jia, G. Yin, J. Zhang, Rotating Ring-Disk Electrode Method, in: Rotating Electrode Methods Oxyg. Reduct. Electrocatalysts, Elsevier, 2014: pp. 199–229. https://doi.org/10.1016/B978-0-444-63278-4.00006-9.
[33] R. Zhou, Y. Zheng, M. Jaroniec, S.-Z. Qiao, Determination of the Electron Transfer Number for the Oxygen Reduction Reaction: From Theory to Experiment, ACS Catal. 6 (2016) 4720–4728. https://doi.org/10.1021/acscatal.6b01581.
[34] S.V. Vassilev, D. Baxter, L.K. Andersen, C.G. Vassileva, An overview of the chemical composition of biomass, Fuel. 89 (2010) 913–933. https://doi.org/10.1016/j.fuel.2009.10.022.
[35] X. Wu, K. Chen, Z. Lin, Y. Zhang, H. Meng, Nitrogen doped graphitic carbon from biomass as non noble metal catalyst for oxygen reduction reaction, Mater. Today Energy. 13 (2019) 100–108. https://doi.org/10.1016/j.mtener.2019.05.004.
[36] D. Mondal, M. Sharma, C.-H. Wang, Y.-C. Lin, H.-C. Huang, A. Saha, et al., Deep eutectic solvent promoted one step sustainable conversion of fresh seaweed biomass to functionalized graphene as a potential electrocatalyst, Green Chem. 18 (2016) 2819–2826. https://doi.org/10.1039/C5GC03106K.
[37] M.Y. Song, H.Y. Park, D.-S. Yang, D. Bhattacharjya, J.-S. Yu, Seaweed-Derived Heteroatom-Doped Highly Porous Carbon as an Electrocatalyst for the Oxygen Reduction Reaction, ChemSusChem. 7 (2014) 1755–1763. https://doi.org/10.1002/cssc.201400049.
[38] X. Liu, Y. Zhou, W. Zhou, L. Li, S. Huang, S. Chen, Biomass-derived nitrogen self-doped porous carbon as effective metal-free catalysts for oxygen reduction reaction, Nanoscale. 7 (2015) 6136–6142. https://doi.org/10.1039/C5NR00013K.
[39] Y. Zhao, Y. Liu, Y. Chen, X. Liu, X. Li, S. Gao, A treasure map for nonmetallic catalysts: optimal nitrogen and fluorine distribution of biomass-derived carbon materials for high-performance oxygen reduction catalysts, J. Mater. Chem. A. 9 (2021) 18251–18259. https://doi.org/10.1039/D1TA05485F.
[40] J. Tang, Y. Wang, W. Zhao, R.J. Zeng, T. Liu, S. Zhou, Biomass-derived hierarchical honeycomb-like porous carbon tube catalyst for the metal-free oxygen reduction reaction, J. Electroanal. Chem. 847 (2019) 113230. https://doi.org/10.1016/j.jelechem.2019.113230.
[41] W. Cao, B. Wang, Y. Xia, W. Zhou, J. Zhang, R. Wen, et al., Preparation of Highly-Active Oxygen Reduction Reaction Catalyst by Direct Co-Pyrolysis of Biomass with KOH, Int. J. Electrochem. Sci. (2019) 250–261. https://doi.org/10.20964/2019.01.33.
[42] Y. Liu, M. Su, D. Li, S. Li, X. Li, J. Zhao, et al., Soybean straw biomass-derived Fe–N co-doped porous carbon as an efficient electrocatalyst for oxygen reduction in both alkaline and acidic media, RSC Adv. 10 (2020) 6763–6771. https://doi.org/10.1039/C9RA07539A.
[43] W. Yuan, A. Xie, S. Li, F. Huang, P. Zhang, Y. Shen, High-activity oxygen reduction catalyst based on low-cost bagasse, nitrogen and large specific surface area, Energy. 115 (2016) 397–403. https://doi.org/10.1016/j.energy.2016.09.026.
[44] R. Wang, K. Wang, Z. Wang, H. Song, H. Wang, S. Ji, Pig bones derived N-doped carbon with multi-level pores as electrocatalyst for oxygen reduction, J. Power Sources. 297 (2015) 295–301. https://doi.org/10.1016/j.jpowsour.2015.07.107.

[45] H. Wang, K. Wang, H. Song, H. Li, S. Ji, Z. Wang, et al., N-doped porous carbon material made from fish-bones and its highly electrocatalytic performance in the oxygen reduction reaction, RSC Adv. 5 (2015) 48965–48970. https://doi.org/10.1039/C5RA09144F.

[46] J. Lee, H.S. Kim, J.-H. Jang, E.-H. Lee, H.-W. Jeong, K.-S. Lee, et al., Atomic-Scale Engineered Fe Single-Atom Electrocatalyst Based on Waste Pig Blood for High-Performance AEMFCs, ACS Sustain. Chem. Eng. 9 (2021) 7863–7872. https://doi.org/10.1021/acssuschemeng.1c01590.

[47] J. Lee, Y. Sohn, S. Kim, J. Min, D. Kim, S.-H. Lee, et al., Insight on the treatment of pig blood as biomass derived electrocatalyst precursor for high performance in the oxygen reduction reaction, Appl. Surf. Sci. 545 (2021) 148940. https://doi.org/10.1016/j.apsusc.2021.148940.

[48] N.K. Chaudhari, M.Y. Song, J.-S. Yu, Heteroatom-doped highly porous carbon from human urine, Sci. Rep. 4 (2015) 5221. https://doi.org/10.1038/srep05221.

[49] K.N. Chaudhari, M.Y. Song, J.-S. Yu, Transforming Hair into Heteroatom-Doped Carbon with High Surface Area, Small. 10 (2014) 2625–2636. https://doi.org/10.1002/smll.201303831.

[50] I.L. Alonso-Lemus, F.J. Rodriguez-Varela, M.Z. Figueroa-Torres, M.E. Sanchez-Castro, A. Hernandez-Ramírez, D. Lardizabal-Gutierrez, et al., Novel self-nitrogen-doped porous carbon from waste leather as highly active metal-free electrocatalyst for the ORR, Int. J. Hydrog. Energy. 41 (2016) 23409–23416. https://doi.org/10.1016/j.ijhydene.2016.09.033.

[51] S. Gao, H. Fan, S. Zhang, Nitrogen-enriched carbon from bamboo fungus with superior oxygen reduction reaction activity, J Mater Chem A. 2 (2014) 18263–18270. https://doi.org/10.1039/C4TA03558E.

[52] C. Guo, W. Liao, Z. Li, L. Sun, C. Chen, Easy conversion of protein-rich enoki mushroom biomass to a nitrogen-doped carbon nanomaterial as a promising metal-free catalyst for oxygen reduction reaction, Nanoscale. 7 (2015) 15990–15998. https://doi.org/10.1039/C5NR03828F.

[53] G. Chen, K. Li, Z. Wu, F. Lin, C. Shen, B. Yan, Agaricus bisporus residue-derived Fe/N co-doped carbon materials as an efficient electrocatalyst for oxygen reduction reaction, Int. J. Hydrog. Energy. 46 (2021) 34737–34748. https://doi.org/10.1016/j.ijhydene.2021.08.059.

[54] X. Wang, W. Ai, N. Li, T. Yu, P. Chen, Graphene–bacteria composite for oxygen reduction and lithium ion batteries, J. Mater. Chem. A. 3 (2015) 12873–12879. https://doi.org/10.1039/C5TA01987G.

[55] L. Wei, D. Yu, H.E. Karahan, Ö. Birer, K. Goh, Y. Yuan, et al., E. coli-derived carbon with nitrogen and phosphorus dual functionalities for oxygen reduction reaction, Catal. Today. 249 (2015) 228–235. https://doi.org/10.1016/j.cattod.2014.08.031.

[56] Z. Guo, G. Ren, C. Jiang, X. Lu, Y. Zhu, L. Jiang, et al., High Performance Heteroatoms Quaternary-doped Carbon Catalysts Derived from Shewanella Bacteria for Oxygen Reduction, Sci. Rep. 5 (2015) 17064. https://doi.org/10.1038/srep17064.

[57] H. Zhu, J. Yin, X. Wang, H. Wang, X. Yang, Microorganism-Derived Heteroatom-Doped Carbon Materials for Oxygen Reduction and Supercapacitors, Adv. Funct. Mater. 23 (2013) 1305–1312. https://doi.org/10.1002/adfm.201201643.

[58] C. Satgé, Etude de nouvelles stratégies de valorisation de mono et polysaccharides = Study of new strategies for the valorization of mono and polysaccharides, Limoges, 2002. http://aurore.unilim.fr/ori-oai-search/notice/view/unilim-ori-11640 (accessed January 12, 2022).

[59] P. Colonna, Produits biosourcés issus des ressources végétales, Chim. Verte. (2019). https://doi.org/10.51257/a-v1-chv600.

[60] R.J. Stoklosa, D.B. Hodge, Integration of (Hemi)-Cellulosic Biofuels Technologies with Chemical Pulp Production, in: Biorefineries, Elsevier, 2014: pp. 73–100. https://doi.org/10.1016/B978-0-444-59498-3.00004-X.

[61] V. Dhyani, T. Bhaskar, A comprehensive review on the pyrolysis of lignocellulosic biomass, Renew. Energy. 129 (2018) 695–716. https://doi.org/10.1016/j.renene.2017.04.035.

[62] J. Quílez-Bermejo, S. Pérez-Rodríguez, A. Celzard, V. Fierro, Progress in the Use of Biosourced Phenolic Molecules for Electrode Manufacturing, Front. Mater. 9 (2022) 810575. https://doi.org/10.3389/fmats.2022.810575.

[63] J. Quílez-Bermejo, E. Morallón, D. Cazorla-Amorós, Metal-free heteroatom-doped carbon-based catalysts for ORR: A critical assessment about the role of heteroatoms, Carbon. 165 (2020) 434–454. https://doi.org/10.1016/j.carbon.2020.04.068.

[64] J.-C. Li, P.-X. Hou, C. Liu, Heteroatom-Doped Carbon Nanotube and Graphene-Based Electrocatalysts for Oxygen Reduction Reaction, Small. 13 (2017) 1702002. https://doi.org/10.1002/smll.201702002.

[65] J. Liu, P. Song, Z. Ning, W. Xu, Recent Advances in Heteroatom-Doped Metal-Free Electrocatalysts for Highly Efficient Oxygen Reduction Reaction, Electrocatalysis. 6 (2015) 132–147. https://doi.org/10.1007/s12678-014-0243-9.

[66] J.H. Cummings, A.M. Stephen, Carbohydrate terminology and classification, Eur. J. Clin. Nutr. 61 (2007) S5–S18. https://doi.org/10.1038/sj.ejcn.1602936.

[67] M. Rinaudo, Chitin and chitosan: Properties and applications, Prog. Polym. Sci. 31 (2006) 603–632. https://doi.org/10.1016/j.progpolymsci.2006.06.001.

[68] N. Hammi, S. Chen, F. Dumeignil, S. Royer, A. El Kadib, Chitosan as a sustainable precursor for nitrogen-containing carbon nanomaterials: synthesis and uses, Mater. Today Sustain. 10 (2020) 100053. https://doi.org/10.1016/j.mtsust.2020.100053.

[69] M. Brebu, I. Spiridon, Thermal degradation of keratin waste, J. Anal. Appl. Pyrolysis. 91 (2011) 288–295. https://doi.org/10.1016/j.jaap.2011.03.003.

[70] K. Varma, S. Gopi, Biopolymers and their role in medicinal and pharmaceutical applications, in: Biopolym. Their Ind. Appl., Elsevier, 2021: pp. 175–191. https://doi.org/10.1016/B978-0-12-819240-5.00007-9.

[71] Q. Wang, J. Yang, X. Zhou, J. Tang, H. Zhong, M. Jia, et al., N, S Co-Doped Hierarchical Porous Carbon from Antibiotic Bacteria Residues as Anode Materials for Lithium Ion Batteries, J. Electrochem. Soc. 166 (2019) A704–A710. https://doi.org/10.1149/2.0901904jes.

[72] fungus - Annotated classification | Britannica, (n.d.). https://www.britannica.com/science/fungus/Outline-of-classification-of-fungi (accessed October 24, 2022).

[73] Y. Qiao, H. Wang, X. Zhang, P. Jia, T. Shen, X. Hao, et al., Ultrahigh volumetric capacitance biomorphic porous carbon material derived from mold, Mater. Lett. 184 (2016) 252–256. https://doi.org/10.1016/j.matlet.2016.08.081.

[74] G. Wang, H. Peng, X. Qiao, L. Du, X. Li, T. Shu, et al., Biomass-derived porous heteroatom-doped carbon spheres as a high-performance catalyst for the oxygen reduction reaction, Int. J. Hydrog. Energy. 41 (2016) 14101–14110. https://doi.org/10.1016/j.ijhydene.2016.06.023.

[75] R. Ryoo, S.H. Joo, M. Kruk, M. Jaroniec, Ordered Mesoporous Carbons, Adv. Mater. 13 (2001) 677–681. https://doi.org/10.1002/1521-4095(200105)13:9<677::AID-ADMA677>3.0.CO;2-C.

[76] A. Ōya, H. Marsh, Phenomena of catalytic graphitization, J. Mater. Sci. 17 (1982) 309–322. https://doi.org/10.1007/BF00591464.

[77] F. Rodríguez-Reinoso, M. Molina-Sabio, Activated carbons from lignocellulosic materials by chemical and/or physical activation: an overview, Carbon. 30 (1992) 1111–1118. https://doi.org/10.1016/0008-6223(92)90143-K.

[78] E. Pérez-Mayoral, I. Matos, M. Bernardo, I. Fonseca, New and Advanced Porous Carbon Materials in Fine Chemical Synthesis. Emerging Precursors of Porous Carbons, Catalysts. 9 (2019) 133. https://doi.org/10.3390/catal9020133.

[79] J. Wang, P. Nie, B. Ding, S. Dong, X. Hao, H. Dou, et al., Biomass derived carbon for energy storage devices, J. Mater. Chem. A. 5 (2017) 2411–2428. https://doi.org/10.1039/C6TA08742F.

[80] J. Lee, J. Kim, T. Hyeon, Recent Progress in the Synthesis of Porous Carbon Materials, Adv. Mater. 18 (2006) 2073–2094. https://doi.org/10.1002/adma.200501576.

[81] M.-M. Titirici, Robin.J. White, C. Falco, M. Sevilla, Black perspectives for a green future: hydrothermal carbons for environment protection and energy storage, Energy Environ. Sci. 5 (2012) 6796. https://doi.org/10.1039/c2ee21166a.

[82] C. Falco, N. Baccile, M.-M. Titirici, Morphological and structural differences between glucose, cellulose and lignocellulosic biomass derived hydrothermal carbons, Green Chem. 13 (2011) 3273. https://doi.org/10.1039/c1gc15742f.

[83] J. Fang, L. Zhan, Y.S. Ok, B. Gao, Minireview of potential applications of hydrochar derived from hydrothermal carbonization of biomass, J. Ind. Eng. Chem. 57 (2018) 15–21. https://doi.org/10.1016/j.jiec.2017.08.026.

[84] O. Bouchenafa, Mécanosynthèse et matériaux de construction : optimisation et application pour la clinkérisation et la géopolymérisation, thesis, Paris Est, 2019. http://www.theses.fr/2019PESC1003 (accessed January 27, 2022).

[85] C.M. Cova, R. Luque, Advances in mechanochemical processes for biomass valorization, BMC Chem. Eng. 1 (2019) 16. https://doi.org/10.1186/s42480-019-0015-7.

[86] P. Baláž, M. Achimovičová, M. Baláž, P. Billik, Z. Cherkezova-Zheleva, J.M. Criado, et al., Hallmarks of mechanochemistry: from nanoparticles to technology, Chem. Soc. Rev. 42 (2013) 7571. https://doi.org/10.1039/c3cs35468g.

[87] J. Castro-Gutiérrez, A. Sanchez-Sanchez, J. Ghanbaja, N. Díez, M. Sevilla, A. Celzard, et al., Synthesis of perfectly ordered mesoporous carbons by water-assisted mechanochemical self-assembly of tannin, Green Chem. 20 (2018) 5123–5132. https://doi.org/10.1039/C8GC02295J.

[88] J. Castro-Gutiérrez, N. Díez, M. Sevilla, M.T. Izquierdo, J. Ghanbaja, A. Celzard, et al., High-Rate Capability of Supercapacitors Based on Tannin-Derived Ordered Mesoporous Carbons, ACS Sustain. Chem. Eng. 7 (2019) 17627–17635. https://doi.org/10.1021/acssuschemeng.9b03407.

[89] L. Xie, Z. Jin, Z. Dai, Y. Chang, X. Jiang, H. Wang, Porous carbons synthesized by templating approach from fluid precursors and their applications in environment and energy storage: A review, Carbon. 170 (2020) 100–118. https://doi.org/10.1016/j.carbon.2020.07.034.

[90] K.L. Yeung, W. Han, Zeolites and mesoporous materials in fuel cell applications, Catal. Today. 236 (2014) 182–205. https://doi.org/10.1016/j.cattod.2013.10.022.

[91] Y. He, Q. Tan, L. Lu, J. Sokolowski, G. Wu, Metal-Nitrogen-Carbon Catalysts for Oxygen Reduction in PEM Fuel Cells: Self-Template Synthesis Approach to Enhancing Catalytic Activity and Stability, Electrochem. Energy Rev. 2 (2019) 231–251. https://doi.org/10.1007/s41918-019-00031-9.

[92] P. Zhang, F. Sun, Z. Xiang, Z. Shen, J. Yun, D. Cao, ZIF-derived in situ nitrogen-doped porous carbons as efficient metal-free electrocatalysts for oxygen reduction reaction, Energy Env. Sci. 7 (2014) 442–450. https://doi.org/10.1039/C3EE42799D.

[93] R. Ruiz-Rosas, M.J. Valero-Romero, D. Salinas-Torres, J. Rodríguez-Mirasol, T. Cordero, E. Morallón, et al., Electrochemical Performance of Hierarchical Porous Carbon Materials Obtained from the Infiltration of Lignin into Zeolite Templates, ChemSusChem. 7 (2014) 1458–1467. https://doi.org/10.1002/cssc.201301408.

[94] Y.-S. Jun, W.H. Hong, M. Antonietti, A. Thomas, Mesoporous, 2D Hexagonal Carbon Nitride and Titanium Nitride/Carbon Composites, Adv. Mater. 21 (2009) 4270–4274. https://doi.org/10.1002/adma.200803500.

[95] J. Quílez-Bermejo, E. Morallón, D. Cazorla-Amorós, Polyaniline-Derived N-Doped Ordered Mesoporous Carbon Thin Films: Efficient Catalysts towards Oxygen Reduction Reaction, Polymers. 12 (2020) 2382. https://doi.org/10.3390/polym12102382.

[96] C. Liang, Z. Li, S. Dai, Mesoporous Carbon Materials: Synthesis and Modification, Angew. Chem. Int. Ed. 47 (2008) 3696–3717. https://doi.org/10.1002/anie.200702046.

[97] F.L. Braghiroli, V. Fierro, J. Parmentier, A. Pasc, A. Celzard, Easy and eco-friendly synthesis of ordered mesoporous carbons by self-assembly of tannin with a block copolymer, Green Chem. 18 (2016) 3265–3271. https://doi.org/10.1039/C5GC02788H.

[98] W. Ma, J. Zhu, Z. Wang, W. Song, G. Cao, Recent advances in preparation and application of laser-induced graphene in energy storage devices, Mater. Today Energy. 18 (2020) 100569. https://doi.org/10.1016/j.mtener.2020.100569.

[99] H.-C. Kuo, Y.-G. Lin, C.-L. Chiang, S.-H. Liu, FeN@N-doped graphitic biochars derived from hydrothermal-microwave pyrolysis of cellulose biomass for fuel cell catalysts, J. Anal. Appl. Pyrolysis. 153 (2021) 104991. https://doi.org/10.1016/j.jaap.2020.104991.

[100] H.-C. Kuo, S.-H. Liu, Y.-G. Lin, C.-L. Chiang, D.C.W. Tsang, Synthesis of FeCo–N@N-doped carbon oxygen reduction catalysts *via* microwave-assisted ammoxidation, Catal. Sci. Technol. 10 (2020) 3949–3958. https://doi.org/10.1039/D0CY00376J.

[101] C. Liedel, Sustainable Battery Materials from Biomass, ChemSusChem. 13 (2020) 2110–2141. https://doi.org/10.1002/cssc.201903577.

[102] H. Lu, X.S. Zhao, Biomass-derived carbon electrode materials for supercapacitors, Sustain. Energy Fuels. 1 (2017) 1265–1281. https://doi.org/10.1039/C7SE00099E.

[103] J. Quílez-Bermejo, M. Melle-Franco, E. San-Fabián, E. Morallón, D. Cazorla-Amorós, Towards understanding the active sites for the ORR in N-doped carbon materials through fine-tuning of nitrogen functionalities: an experimental and computational approach, J. Mater. Chem. A. 7 (2019) 24239–24250. https://doi.org/10.1039/C9TA07932G.

[104] J. Quílez-Bermejo, K. Strutyński, M. Melle-Franco, E. Morallón, D. Cazorla-Amorós, On the Origin of the Effect of pH in Oxygen Reduction Reaction for Nondoped and Edge-Type Quaternary N-Doped Metal-Free Carbon-Based Catalysts, ACS Appl. Mater. Interfaces. 12 (2020) 54815–54823. https://doi.org/10.1021/acsami.0c17249.

[105] J. Quílez-Bermejo, C. González-Gaitán, E. Morallón, D. Cazorla-Amorós, Effect of carbonization conditions of polyaniline on its catalytic activity towards ORR. Some insights about the nature of the active sites, Carbon. 119 (2017) 62–71. https://doi.org/10.1016/j.carbon.2017.04.015.

[106] X. Feng, Y. Bai, M. Liu, Y. Li, H. Yang, X. Wang, et al., Untangling the respective effects of heteroatom-doped carbon materials in batteries, supercapacitors and the ORR to design high performance materials, Energy Environ. Sci. 14 (2021) 2036–2089. https://doi.org/10.1039/D1EE00166C.

[107] L.R. Radovic, Active Sites in Graphene and the Mechanism of CO_2 Formation in Carbon Oxidation, J. Am. Chem. Soc. 131 (2009) 17166–17175. https://doi.org/10.1021/ja904731q.

[108] D. Barrera, M. Florent, K. Sapag, T.J. Bandosz, Insight into the Mechanism of Oxygen Reduction Reaction on Micro/Mesoporous Carbons: Ultramicropores versus Nitrogen-Containing Catalytic Centers in Ordered Pore Structure, ACS Appl. Energy Mater. 2 (2019) 7412–7424. https://doi.org/10.1021/acsaem.9b01427.

[109] J. Encalada, K. Savaram, N.A. Travlou, W. Li, Q. Li, C. Delgado-Sánchez, et al., Combined Effect of Porosity and Surface Chemistry on the Electrochemical Reduction of Oxygen on Cellular Vitreous Carbon Foam Catalyst, ACS Catal. 7 (2017) 7466–7478. https://doi.org/10.1021/acscatal.7b01977.

[110] A. Gabe, R. Ruiz-Rosas, C. González-Gaitán, E. Morallón, D. Cazorla-Amorós, Modeling of oxygen reduction reaction in porous carbon materials in alkaline medium. Effect of microporosity, J. Power Sources. 412 (2019) 451–464. https://doi.org/10.1016/j.jpowsour.2018.11.075.

[111] D. Li, Y. Fan, H. Yuan, L. Deng, J. Yang, Y. Chen, et al., Renewable and Metal-Free Carbon Derived from Aquatic Scindapsus Affording Meso–microporosity, Large Interface, and Enriched Pyridinic-N for Efficient Oxygen Reduction Reaction Catalysis, Energy Fuels. 34 (2020) 13089–13095. https://doi.org/10.1021/acs.energyfuels.0c02246.

[112] H. Zhou, J. Zhang, J. Zhu, Z. Liu, C. Zhang, S. Mu, A self-template and KOH activation co-coupling strategy to synthesize ultrahigh surface area nitrogen-doped porous graphene for oxygen reduction, RSC Adv. 6 (2016) 73292–73300. https://doi.org/10.1039/C6RA16703A.

[113] J. Li, S. Gao, B. Li, Y. Li, C. Cheng, C. Maouche, et al., Biomass-derived nitrogen-doped porous carbons with ultra-high surface area for electrocatalytic oxygen reduction reaction, J. Electroanal. Chem. 878 (2020) 114542. https://doi.org/10.1016/j.jelechem.2020.114542.

[114] K. Kaare, E. Yu, A. Volperts, G. Dobele, A. Zhurinsh, A. Dyck, et al., Highly Active Wood-Derived Nitrogen-Doped Carbon Catalyst for the Oxygen Reduction Reaction, ACS Omega. 5 (2020) 23578–23587. https://doi.org/10.1021/acsomega.0c01974.
[115] L. Yu, C. Yang, W. Zhang, W. Liu, H. Wang, J. Qi, et al., Solvent-free synthesis of N-doped nanoporous carbon materials as durable high-performance pH-universal ORR catalysts, J. Colloid Interface Sci. 575 (2020) 406–415. https://doi.org/10.1016/j.jcis.2020.05.012.
[116] D. He, W. Zhao, P. Li, S. Sun, Q. Tan, K. Han, et al., Bifunctional biomass-derived N, S dual-doped ladder-like porous carbon for supercapacitor and oxygen reduction reaction, J. Alloys Compd. 773 (2019) 11–20. https://doi.org/10.1016/j.jallcom.2018.09.141.
[117] L.R. Radovic, ed., Chemistry & Physics Of Carbon, 0 ed., CRC Press, 2004. https://doi.org/10.1201/9780203997031.
[118] S. Nagappan, M. Duraivel, S.A. Hira, K. Prabakar, C.-S. Ha, S.H. Joo, et al., Heteroatom-doped nanomaterials/core–shell nanostructure based electrocatalysts for the oxygen reduction reaction, J. Mater. Chem. A. 10 (2022) 987–1021. https://doi.org/10.1039/D1TA09861F.
[119] D. Higgins, Z. Chen, Z. Chen, Nitrogen doped carbon nanotubes synthesized from aliphatic diamines for oxygen reduction reaction, Electrochimica Acta. 56 (2011) 1570–1575. https://doi.org/10.1016/j.electacta.2010.11.003.
[120] Z. Chen, D. Higgins, H. Tao, R.S. Hsu, Z. Chen, Highly Active Nitrogen-Doped Carbon Nanotubes for Oxygen Reduction Reaction in Fuel Cell Applications, J. Phys. Chem. C. 113 (2009) 21008–21013. https://doi.org/10.1021/jp908067v.
[121] W. Zhang, J. Qi, P. Bai, H. Wang, L. Xu, High-level nitrogen-doped, micro/mesoporous carbon as an efficient metal-free electrocatalyst for the oxygen reduction reaction: optimizing the reaction surface area by a solvent-free mechanochemical method, New J. Chem. 43 (2019) 10878–10886. https://doi.org/10.1039/C9NJ01997A.
[122] H. Wang, W. Zhang, P. Bai, L. Xu, Ultrasound-assisted transformation from waste biomass to efficient carbon-based metal-free pH-universal oxygen reduction reaction electrocatalysts, Ultrason. Sonochem. 65 (2020) 105048. https://doi.org/10.1016/j.ultsonch.2020.105048.
[123] S.N. Faisal, E. Haque, N. Noorbehesht, W. Zhang, A.T. Harris, T.L. Church, et al., Pyridinic and graphitic nitrogen-rich graphene for high-performance supercapacitors and metal-free bifunctional electrocatalysts for ORR and OER, RSC Adv. 7 (2017) 17950–17958. https://doi.org/10.1039/C7RA01355H.
[124] J.J. Zhang, Y. Sun, L.K. Guo, X.N. Sun, N.B. Huang, Ball-Milling Effect on Biomass-Derived Nanocarbon Catalysts for the Oxygen Reduction Reaction, ChemistrySelect. 6 (2021) 6019–6028. https://doi.org/10.1002/slct.202100752.
[125] J. Quílez-Bermejo, E. Morallón, D. Cazorla-Amorós, On the deactivation of N-doped carbon materials active sites during oxygen reduction reaction, Carbon. 189 (2022) 548–560. https://doi.org/10.1016/j.carbon.2021.12.086.
[126] J. Quílez-Bermejo, S. Pérez-Rodríguez, R. Canevesi, D. Torres, E. Morallón, D. Cazorla-Amorós, et al., Easy enrichment of graphitic nitrogen to prepare highly catalytic carbons for oxygen reduction reaction, Carbon. 196 (2022) 708–717. https://doi.org/10.1016/j.carbon.2022.05.032.
[127] L. Liu, G. Zeng, J. Chen, L. Bi, L. Dai, Z. Wen, N-doped porous carbon nanosheets as pH-universal ORR electrocatalyst in various fuel cell devices, Nano Energy. 49 (2018) 393–402. https://doi.org/10.1016/j.nanoen.2018.04.061.
[128] F. Pan, S. Guo, J. Zhang, Swelling-induced synthesis of nitrogen-doped graphene for oxygen reduction reaction, Electrochimica Acta. 180 (2015) 29–36. https://doi.org/10.1016/j.electacta.2015.08.079.
[129] Q. Zhao, Q. Ma, F. Pan, Z. Wang, B. Yang, J. Zhang, et al., Facile synthesis of nitrogen-doped carbon nanosheets as metal-free catalyst with excellent oxygen reduction performance in alkaline and acidic media, J. Solid State Electrochem. 20 (2016) 1469–1479. https://doi.org/10.1007/s10008-016-3157-z.

[130] Y. Li, H. Zhang, P. Liu, Y. Wang, H. Yang, Y. Li, et al., Self-supported bimodal-pore structured nitrogen-doped carbon fiber aerogel as electrocatalyst for oxygen reduction reaction, Electrochem. Commun. 51 (2015) 6–10. https://doi.org/10.1016/j.elecom.2014.11.020.
[131] R. Liu, H. Zhang, S. Liu, X. Zhang, T. Wu, X. Ge, et al., Shrimp-shell derived carbon nanodots as carbon and nitrogen sources to fabricate three-dimensional N-doped porous carbon electrocatalysts for the oxygen reduction reaction, Phys. Chem. Chem. Phys. 18 (2016) 4095–4101. https://doi.org/10.1039/C5CP06970J.
[132] J. Ma, M. Shi, T.K.A. Hoang, Z. Yao, A. Sun, A facile preparation of nitrogen-doped porous carbons from renewable as efficient catalysts for oxygen reduction reaction, J. Solid State Chem. 291 (2020) 121609. https://doi.org/10.1016/j.jssc.2020.121609.
[133] L. Lai, J.R. Potts, D. Zhan, L. Wang, C.K. Poh, C. Tang, et al., Exploration of the active center structure of nitrogen-doped graphene-based catalysts for oxygen reduction reaction, Energy Environ. Sci. 5 (2012) 7936. https://doi.org/10.1039/c2ee21802j.
[134] J. Liu, P. Song, W. Xu, Structure-activity relationship of doped-nitrogen (N)-based metal-free active sites on carbon for oxygen reduction reaction, Carbon. 115 (2017) 763–772. https://doi.org/10.1016/j.carbon.2017.01.080.
[135] M. Li, H. Zhang, T. Xiao, S. Wang, B. Zhang, D. Chen, et al., Low-cost biochar derived from corncob as oxygen reduction catalyst in air cathode microbial fuel cells, Electrochimica Acta. 283 (2018) 780–788. https://doi.org/10.1016/j.electacta.2018.07.010.
[136] A. Tyagi, S. Banerjee, S. Singh, K.K. Kar, Biowaste derived activated carbon electrocatalyst for oxygen reduction reaction: Effect of chemical activation, Int. J. Hydrog. Energy. 45 (2020) 16930–16943. https://doi.org/10.1016/j.ijhydene.2019.06.195.
[137] A. Tyagi, A. Yadav, P. Sinha, S. Singh, P. Paik, K.K. Kar, Chicken feather rachis: An improvement over feather fiber derived electrocatalyst for oxygen electroreduction, Appl. Surf. Sci. 495 (2019) 143603. https://doi.org/10.1016/j.apsusc.2019.143603.
[138] Y. Gao, Q. Wang, G. Ji, A. Li, J. Niu, Doping strategy, properties and application of heteroatom-doped ordered mesoporous carbon, RSC Adv. 11 (2021) 5361–5383. https://doi.org/10.1039/D0RA08993A.
[139] X. Li, Y. Fang, S. Zhao, J. Wu, F. Li, M. Tian, et al., Nitrogen-doped mesoporous carbon nanosheet/carbon nanotube hybrids as metal-free bi-functional electrocatalysts for water oxidation and oxygen reduction, J. Mater. Chem. A. 4 (2016) 13133–13141. https://doi.org/10.1039/C6TA04187F.
[140] T.-N. Ye, L.-B. Lv, X.-H. Li, M. Xu, J.-S. Chen, Strongly Veined Carbon Nanoleaves as a Highly Efficient Metal-Free Electrocatalyst, Angew. Chem. 126 (2014) 7025–7029. https://doi.org/10.1002/ange.201403363.
[141] P. Chen, L.-K. Wang, G. Wang, M.-R. Gao, J. Ge, W.-J. Yuan, et al., Nitrogen-doped nanoporous carbon nanosheets derived from plant biomass: an efficient catalyst for oxygen reduction reaction, Energy Env. Sci. 7 (2014) 4095–4103. https://doi.org/10.1039/C4EE02531H.
[142] P. Fu, L. Zhou, L. Sun, B. Huang, Y. Yuan, Nitrogen-doped porous activated carbon derived from cocoon silk as a highly efficient metal-free electrocatalyst for the oxygen reduction reaction, RSC Adv. 7 (2017) 13383–13389. https://doi.org/10.1039/C7RA00433H.
[143] R. Li, X. Shao, S. Li, P. Cheng, Z. Hu, D. Yuan, Metal-free N-doped carbon nanofibers as an efficient catalyst for oxygen reduction reactions in alkaline and acid media, Nanotechnology. 27 (2016) 505402. https://doi.org/10.1088/0957-4484/27/50/505402.
[144] J. Liu, L. Wei, H. Wang, G. Lan, H. Yang, J. Shen, Biomass-derived N-doped porous activated carbon as a high-performance and cost-effective pH-universal oxygen reduction catalyst in fuel cell, Int. J. Hydrog. Energy. 45 (2020) 29308–29321. https://doi.org/10.1016/j.ijhydene.2020.07.216.
[145] H. Zheng, Y. Zhang, J. Long, R. Li, X. Gou, Nitrogen-Doped Porous Carbon Material Derived from Biomass of Beancurd as an Efficient Electrocatalyst for Oxygen Reduction and Zn-air Fuel Cell, J. Electrochem. Soc. 167 (2020) 084516. https://doi.org/10.1149/1945-7111/ab907f.

[146] X. Liu, L. Li, W. Zhou, Y. Zhou, W. Niu, S. Chen, High-Performance Electrocatalysts for Oxygen Reduction Based on Nitrogen-Doped Porous Carbon from Hydrothermal Treatment of Glucose and Dicyandiamide, ChemElectroChem. 2 (2015) 803–810. https://doi.org/10.1002/celc.201500002.
[147] M.K. Rybarczyk, M. Lieder, M. Jablonska, N-doped mesoporous carbon nanosheets obtained by pyrolysis of a chitosan–melamine mixture for the oxygen reduction reaction in alkaline media, RSC Adv. 5 (2015) 44969–44977. https://doi.org/10.1039/C5RA05725F.
[148] C. Guo, X. Tong, X.-Y. Guo, Nitrogen-doped mesoporous network-like carbon as an efficient metal-free electrocatalyst for oxygen reduction reaction, Int. J. Hydrog. Energy. 41 (2016) 22941–22951. https://doi.org/10.1016/j.ijhydene.2016.10.043.
[149] I.L. Alonso-Lemus, B. Escobar-Morales, D. Lardizabal-Gutierrez, L. de la Torre-Saenz, P. Quintana-Owen, F.J. Rodriguez-Varela, Short communication: Onion skin waste-derived biocarbon as alternative non-noble metal electrocatalyst towards ORR in alkaline media, Int. J. Hydrog. Energy. 44 (2019) 12409–12414. https://doi.org/10.1016/j.ijhydene.2018.10.050.
[150] Y. Zhang, L. Deng, H. Hu, Y. Qiao, H. Yuan, D. Chen, et al., Pomelo peel-derived, N-doped biochar microspheres as an efficient and durable metal-free ORR catalyst in microbial fuel cells, Sustain. Energy Fuels. 4 (2020) 1642–1653. https://doi.org/10.1039/C9SE00834A.
[151] S. Gao, H. Fan, Y. Chen, L. Li, Y. Bando, D. Golberg, One stone, two birds: Gastrodia elata-derived heteroatom-doped carbon materials for efficient oxygen reduction electrocatalyst and as fluorescent decorative materials, Nano Energy. 2 (2013) 1261–1270. https://doi.org/10.1016/j.nanoen.2013.06.005.
[152] X. Yang, K. Li, J. Lv, X. Chen, H.-Y. Zang, H.-Q. Tan, et al., N-doped Hierarchical Porous Carbon Nanomeshes as Oxygen Reduction in pH-Universal Media and Oxygen Evolution Electrocatalysts, ChemElectroChem. 5 (2018) 3279–3286. https://doi.org/10.1002/celc.201800813.
[153] F. Pan, Z. Cao, Q. Zhao, H. Liang, J. Zhang, Nitrogen-doped porous carbon nanosheets made from biomass as highly active electrocatalyst for oxygen reduction reaction, J. Power Sources. 272 (2014) 8–15. https://doi.org/10.1016/j.jpowsour.2014.07.180.
[154] K. Kaare, E. Yu, T. Käämbre, A. Volperts, G. Dobele, A. Zhurinsh, et al., Biomass-derived Graphene-like Catalyst Material for Oxygen Reduction Reaction, ChemNanoMat. 7 (2021) 307–313. https://doi.org/10.1002/cnma.202000615.
[155] S. Gao, X. Li, L. Li, X. Wei, A versatile biomass derived carbon material for oxygen reduction reaction, supercapacitors and oil/water separation, Nano Energy. 33 (2017) 334–342. https://doi.org/10.1016/j.nanoen.2017.01.045.
[156] R. Rajendiran, M. Nallal, K.H. Park, O.L. Li, H.-J. Kim, K. Prabakar, Mechanochemical assisted synthesis of heteroatoms inherited highly porous carbon from biomass for electrochemical capacitor and oxygen reduction reaction electrocatalysis, Electrochimica Acta. 317 (2019) 1–9. https://doi.org/10.1016/j.electacta.2019.05.139.
[157] G. Lin, R. Ma, Y. Zhou, Q. Liu, X. Dong, J. Wang, KOH activation of biomass-derived nitrogen-doped carbons for supercapacitor and electrocatalytic oxygen reduction, Electrochimica Acta. 261 (2018) 49–57. https://doi.org/10.1016/j.electacta.2017.12.107.
[158] Y. Sun, J. Wu, J. Tian, C. Jin, R. Yang, Sulfur-doped carbon spheres as efficient metal-free electrocatalysts for oxygen reduction reaction, Electrochimica Acta. 178 (2015) 806–812. https://doi.org/10.1016/j.electacta.2015.08.059.
[159] T. Sun, J. Wang, C. Qiu, X. Ling, B. Tian, W. Chen, et al., B, N Codoped and Defect-Rich Nanocarbon Material as a Metal-Free Bifunctional Electrocatalyst for Oxygen Reduction and Evolution Reactions, Adv. Sci. 5 (2018) 1800036. https://doi.org/10.1002/advs.201800036.
[160] L. Zhang, J. Niu, M. Li, Z. Xia, Catalytic Mechanisms of Sulfur-Doped Graphene as Efficient Oxygen Reduction Reaction Catalysts for Fuel Cells, J. Phys. Chem. C. 118 (2014) 3545–3553. https://doi.org/10.1021/jp410501u.

[161] J. Wu, C. Jin, Z. Yang, J. Tian, R. Yang, Synthesis of phosphorus-doped carbon hollow spheres as efficient metal-free electrocatalysts for oxygen reduction, Carbon. 82 (2015) 562–571. https://doi.org/10.1016/j.carbon.2014.11.008.
[162] H. Wang, H. Wang, Y. Chen, Y. Liu, J. Zhao, Q. Cai, et al., Phosphorus-doped graphene and (8, 0) carbon nanotube: Structural, electronic, magnetic properties, and chemical reactivity, Appl. Surf. Sci. 273 (2013) 302–309. https://doi.org/10.1016/j.apsusc.2013.02.035.
[163] X. Zhang, Z. Lu, Z. Fu, Y. Tang, D. Ma, Z. Yang, The mechanisms of oxygen reduction reaction on phosphorus doped graphene: A first-principles study, J. Power Sources. 276 (2015) 222–229. https://doi.org/10.1016/j.jpowsour.2014.11.105.
[164] Y. Li, J. Yang, J. Huang, Y. Zhou, K. Xu, N. Zhao, et al., Soft template-assisted method for synthesis of nitrogen and sulfur co-doped three-dimensional reduced graphene oxide as an efficient metal free catalyst for oxygen reduction reaction, Carbon. 122 (2017) 237–246. https://doi.org/10.1016/j.carbon.2017.06.046.
[165] L.R. Radovic, B. Bockrath, On the Chemical Nature of Graphene Edges: Origin of Stability and Potential for Magnetism in Carbon Materials, J. Am. Chem. Soc. 127 (2005) 5917–5927. https://doi.org/10.1021/ja050124h.
[166] S. Gao, L. Li, K. Geng, X. Wei, S. Zhang, Recycling the biowaste to produce nitrogen and sulfur self-doped porous carbon as an efficient catalyst for oxygen reduction reaction, Nano Energy. 16 (2015) 408–418. https://doi.org/10.1016/j.nanoen.2015.07.009.
[167] S. Gao, H. Liu, K. Geng, X. Wei, Honeysuckles-derived porous nitrogen, sulfur, dual-doped carbon as high-performance metal-free oxygen electroreduction catalyst, Nano Energy. 12 (2015) 785–793. https://doi.org/10.1016/j.nanoen.2015.02.004.
[168] I.S. Amiinu, J. Zhang, Z. Kou, X. Liu, O.K. Asare, H. Zhou, et al., Self-Organized 3D Porous Graphene Dual-Doped with Biomass-Sponsored Nitrogen and Sulfur for Oxygen Reduction and Evolution, ACS Appl. Mater. Interfaces. 8 (2016) 29408–29418. https://doi.org/10.1021/acsami.6b08719.
[169] B. Zhang, R. Chen, Z. Yang, Y. Chen, L. Zhou, Y. Yuan, Rapeseed meal-based autochthonous N and S-doped non-metallic porous carbon electrode material for oxygen reduction reaction catalysis, Int. J. Hydrog. Energy. 46 (2021) 508–517. https://doi.org/10.1016/j.ijhydene.2020.09.198.
[170] J. Liang, Y. Jiao, M. Jaroniec, S.Z. Qiao, Sulfur and Nitrogen Dual-Doped Mesoporous Graphene Electrocatalyst for Oxygen Reduction with Synergistically Enhanced Performance, Angew. Chem. Int. Ed. 51 (2012) 11496–11500. https://doi.org/10.1002/anie.201206720.
[171] H.T. Larijani, M. Khorshidian, Theoretical insight into the role of pyridinic nitrogen on the catalytic activity of boron-doped graphene towards oxygen reduction reaction, Appl. Surf. Sci. 492 (2019) 826–842. https://doi.org/10.1016/j.apsusc.2019.05.149.
[172] Y. Shen, F. Peng, Y. Cao, J. Zuo, H. Wang, H. Yu, Preparation of nitrogen and sulfur co-doped ultrathin graphitic carbon via annealing bagasse lignin as potential electrocatalyst towards oxygen reduction reaction in alkaline and acid media, J. Energy Chem. 34 (2019) 33–42. https://doi.org/10.1016/j.jechem.2018.09.021.
[173] L. Song, J. Chang, Y. Ma, W. Jiang, Y. Xu, C. Liang, et al., Biomass-derived nitrogen and sulfur co-doped carbon microtubes for the oxygen reduction reaction, Mater. Chem. Front. 4 (2020) 3251–3257. https://doi.org/10.1039/D0QM00423E.
[174] Y. Wang, Y. Lei, H. Wang, Astridia velutina-like S, N-codoped hierarchical porous carbon from silk cocoon for superior oxygen reduction reaction, RSC Adv. 6 (2016) 73560–73565. https://doi.org/10.1039/C6RA06664J.
[175] J. Zhang, J. He, H. Zheng, R. Li, X. Gou, N,S dual-doped carbon nanosheet networks with hierarchical porosity derived from biomass of Allium cepa as efficient catalysts for oxygen reduction and Zn–air batteries, J. Mater. Sci. 55 (2020) 7464–7476. https://doi.org/10.1007/s10853-020-04535-4.

[176] Y. Gao, D. Kong, J. Liang, D. Han, B. Wang, Q.-H. Yang, et al., Inside-out dual-doping effects on tubular catalysts: Structural and chemical variation for advanced oxygen reduction performance, Nano Res. 15 (2022) 361–367. https://doi.org/10.1007/s12274-021-3484-y.
[177] G. Zhao, L. Shi, J. Xu, X. Yan, T.S. Zhao, Role of phosphorus in nitrogen, phosphorus dual-doped ordered mesoporous carbon electrocatalyst for oxygen reduction reaction in alkaline media, Int. J. Hydrog. Energy. 43 (2018) 1470–1478. https://doi.org/10.1016/j.ijhydene.2017.11.165.
[178] C. Cao, L. Wei, Q. Zhai, G. Wang, J. Shen, Biomass-derived nitrogen and boron dual-doped hollow carbon tube as cost-effective and stable synergistic catalyst for oxygen electroreduction, Electrochimica Acta. 249 (2017) 328–336. https://doi.org/10.1016/j.electacta.2017.08.025.
[179] Y. Zheng, Y. Jiao, L. Ge, M. Jaroniec, S.Z. Qiao, Two-Step Boron and Nitrogen Doping in Graphene for Enhanced Synergistic Catalysis, Angew. Chem. 125 (2013) 3192–3198. https://doi.org/10.1002/ange.201209548.
[180] H. Wang, J. Sun, J. Wang, L. Jiang, H. Liu, Green synthesis of nitrogen and fluorine co-doped porous carbons from sustainable coconut shells as an advanced synergistic electrocatalyst for oxygen reduction, J. Mater. Res. Technol. 13 (2021) 962–970. https://doi.org/10.1016/j.jmrt.2021.05.048.
[181] H. Zhou, Y. Peng, H.B. Wu, F. Sun, H. Yu, F. Liu, et al., Fluorine-rich nanoporous carbon with enhanced surface affinity in organic electrolyte for high-performance supercapacitors, Nano Energy. 21 (2016) 80–89. https://doi.org/10.1016/j.nanoen.2015.12.016.
[182] S.G. Peera, A.K. Sahu, A. Arunchander, S.D. Bhat, J. Karthikeyan, P. Murugan, Nitrogen and fluorine co-doped graphite nanofibers as high durable oxygen reduction catalyst in acidic media for polymer electrolyte fuel cells, Carbon. 93 (2015) 130–142. https://doi.org/10.1016/j.carbon.2015.05.002.
[183] S. Sadeghhassani, L. Samiee, M.R. Ganjali, A.M. Rashidi, Facile and economic synthesis of heteroatoms co-doped graphene using garlic biomass as a highly stable electrocatalyst toward 4 e− ORR, J. Iran. Chem. Soc. 19 (2022) 257–267. https://doi.org/10.1007/s13738-021-02306-9.
[184] Y. Shen, Y. Li, G. Yang, Q. Zhang, H. Liang, F. Peng, Lignin derived multi-doped (N, S, Cl) carbon materials as excellent electrocatalyst for oxygen reduction reaction in proton exchange membrane fuel cells, J. Energy Chem. 44 (2020) 106–114. https://doi.org/10.1016/j.jechem.2019.09.019.
[185] N. Huang, J. Zhang, Y. Sun, X. Sun, Z. Qiu, X. Ge, A non-traditional biomass-derived N, P, and S ternary self-doped 3D multichannel carbon ORR electrocatalyst, New J. Chem. 44 (2020) 14604–14614. https://doi.org/10.1039/D0NJ03283B.
[186] J. Zhang, H. Zhou, X. Liu, J. Zhang, T. Peng, J. Yang, et al., Keratin-derived S/N co-doped graphene-like nanobubble and nanosheet hybrids for highly efficient oxygen reduction, J. Mater. Chem. A. 4 (2016) 15870–15879. https://doi.org/10.1039/C6TA06212A.
[187] M. Zhang, Y. Song, H. Tao, C. Yan, J. Masa, Y. Liu, et al., Lignosulfonate biomass derived N and S co-doped porous carbon for efficient oxygen reduction reaction, Sustain. Energy Fuels. 2 (2018) 1820–1827. https://doi.org/10.1039/C8SE00231B.
[188] X. Zhang, D. Yu, Y. Zhang, W. Guo, X. Ma, X. He, Nitrogen- and sulfur-doped carbon nanoplatelets via thermal annealing of alkaline lignin with urea as efficient electrocatalysts for oxygen reduction reaction, RSC Adv. 6 (2016) 104183–104192. https://doi.org/10.1039/C6RA21958F.
[189] D.M. Fernandes, A.S. Mestre, A. Martins, N. Nunes, A.P. Carvalho, C. Freire, Biomass-derived nanoporous carbons as electrocatalysts for oxygen reduction reaction, Catal. Today. 357 (2020) 269–278. https://doi.org/10.1016/j.cattod.2019.02.048.
[190] T.X. Wu, G.Z. Wang, X. Zhang, C. Chen, Y.X. Zhang, H.J. Zhao, Transforming chitosan into N-doped graphitic carbon electrocatalysts, Chem. Commun. 51 (2015) 1334–1337. https://doi.org/10.1039/C4CC09355K.

[191] B. Zheng, J. Wang, Z. Pan, X. Wang, S. Liu, S. Ding, et al., An efficient metal-free catalyst derived from waste lotus seedpod for oxygen reduction reaction, J. Porous Mater. 27 (2020) 637–646. https://doi.org/10.1007/s10934-019-00846-3.
[192] A. Mulyadi, Z. Zhang, M. Dutzer, W. Liu, Y. Deng, Facile approach for synthesis of doped carbon electrocatalyst from cellulose nanofibrils toward high-performance metal-free oxygen reduction and hydrogen evolution, Nano Energy. 32 (2017) 336–346. https://doi.org/10.1016/j.nanoen.2016.12.057.
[193] L. Han, X. Cui, Y. Liu, G. Han, X. Wu, C. (Charles) Xu, et al., Nitrogen and phosphorus modification to enhance the catalytic activity of biomass-derived carbon toward the oxygen reduction reaction, Sustain. Energy Fuels. 4 (2020) 2707–2717. https://doi.org/10.1039/C9SE00985J.
[194] M. Borghei, N. Laocharoen, E. Kibena-Põldsepp, L.-S. Johansson, J. Campbell, E. Kauppinen, et al., Porous N,P-doped carbon from coconut shells with high electrocatalytic activity for oxygen reduction: Alternative to Pt-C for alkaline fuel cells, Appl. Catal. B Environ. 204 (2017) 394–402. https://doi.org/10.1016/j.apcatb.2016.11.029.
[195] F. Liu, H. Peng, X. Qiao, Z. Fu, P. Huang, S. Liao, High-performance doped carbon electrocatalyst derived from soybean biomass and promoted by zinc chloride, Int. J. Hydrog. Energy. 39 (2014) 10128–10134. https://doi.org/10.1016/j.ijhydene.2014.04.176.
[196] L. Xu, H. Fan, L. Huang, J. Xia, S. Li, M. Li, et al., Chrysanthemum-derived N and S co-doped porous carbon for efficient oxygen reduction reaction and aluminum-air battery, Electrochimica Acta. 239 (2017) 1–9. https://doi.org/10.1016/j.electacta.2017.04.002.
[197] Z.R. Ismagilov, A.E. Shalagina, O.Yu. Podyacheva, A.V. Ischenko, L.S. Kibis, A.I. Boronin, et al., Structure and electrical conductivity of nitrogen-doped carbon nanofibers, Carbon. 47 (2009) 1922–1929. https://doi.org/10.1016/j.carbon.2009.02.034.
[198] Z. Chen, D. Higgins, A. Yu, L. Zhang, J. Zhang, A review on non-precious metal electrocatalysts for PEM fuel cells, Energy Environ. Sci. 4 (2011) 3167. https://doi.org/10.1039/c0ee00558d.
[199] Y. Li, K. Zang, X. Duan, J. Luo, D. Chen, Boost oxygen reduction reaction performance by tuning the active sites in Fe-N-P-C catalysts, J. Energy Chem. 55 (2021) 572–579. https://doi.org/10.1016/j.jechem.2020.07.041.
[200] Y. Goto, Y. Nakayasu, H. Abe, Y. Katsuyama, T. Itoh, M. Watanabe, Synthesis of unused-wood-derived C-Fe-N catalysts for oxygen reduction reaction by heteroatom doping during hydrothermal carbonization and subsequent carbonization in nitrogen atmosphere, Philos. Trans. R. Soc. Math. Phys. Eng. Sci. 379 (2021) 20200348. https://doi.org/10.1098/rsta.2020.0348.
[201] Q. Lai, Q. Su, Q. Gao, Y. Liang, Y. Wang, Z. Yang, et al., *In Situ* Self-Sacrificed Template Synthesis of Fe-N/G Catalysts for Enhanced Oxygen Reduction, ACS Appl. Mater. Interfaces. 7 (2015) 18170–18178. https://doi.org/10.1021/acsami.5b05834.
[202] D. Li, Y. Qu, S. Li, M. Wei, Y. Liu, A novel honeycomb Fe-N-C composition derived from wheat flour as an efficiency catalyst for the oxygen reduction reaction, J. Solid State Electrochem. 24 (2020) 1105–1112. https://doi.org/10.1007/s10008-020-04578-2.
[203] B. Men, Y. Sun, J. Liu, Y. Tang, Y. Chen, P. Wan, et al., Synergistically Enhanced Electrocatalytic Activity of Sandwich-like N-Doped Graphene/Carbon Nanosheets Decorated by Fe and S for Oxygen Reduction Reaction, ACS Appl. Mater. Interfaces. 8 (2016) 19533–19541. https://doi.org/10.1021/acsami.6b06329.
[204] R. Li, F.-Y. Zheng, X. Zhang, J. Hu, C. Xu, Y. Zhang, Phosphorus and iron doped nitrogen-containing carbon derived from biomass for oxygen reduction under various pH conditions, Int. J. Hydrog. Energy. 45 (2020) 28651–28663. https://doi.org/10.1016/j.ijhydene.2020.07.178.
[205] Y. Zheng, S. Chen, H. Lu, C. Zhang, T. Liu, 3D honeycombed cobalt, nitrogen co-doped carbon nanosheets via hypersaline-protected pyrolysis towards efficient oxygen reduction, Nanotechnology. 31 (2020) 364003. https://doi.org/10.1088/1361-6528/ab97d5.

[206] M. Hao, R. Dun, Y. Su, L. He, F. Ning, X. Zhou, et al., *In situ* self-doped biomass-derived porous carbon as an excellent oxygen reduction electrocatalyst for fuel cells and metal–air batteries, J. Mater. Chem. A. 9 (2021) 14331–14343. https://doi.org/10.1039/D1TA01417J.

[207] H.S. Kim, J. Lee, J.-H. Jang, H. Jin, V.K. Paidi, S.-H. Lee, et al., Waste pig blood-derived 2D Fe single-atom porous carbon as an efficient electrocatalyst for zinc–air batteries and AEMFCs, Appl. Surf. Sci. 563 (2021) 150208. https://doi.org/10.1016/j.apsusc.2021.150208.

[208] C. Zhu, S. Fu, Q. Shi, D. Du, Y. Lin, Single-Atom Electrocatalysts, Angew. Chem. Int. Ed. 56 (2017) 13944–13960. https://doi.org/10.1002/anie.201703864.

[209] L. Zhang, Y. Ren, W. Liu, A. Wang, T. Zhang, Single-atom catalyst: a rising star for green synthesis of fine chemicals, Natl. Sci. Rev. 5 (2018) 653–672. https://doi.org/10.1093/nsr/nwy077.

[210] R. Jasinski, A New Fuel Cell Cathode Catalyst, Nature. 201 (1964) 1212–1213. https://doi.org/10.1038/2011212a0.

[211] E. Yeager, Dioxygen electrocatalysis: mechanisms in relation to catalyst structure, J. Mol. Catal. 38 (1986) 5–25. https://doi.org/10.1016/0304-5102(86)87045-6.

[212] M. Shao, Q. Chang, J.-P. Dodelet, R. Chenitz, Recent Advances in Electrocatalysts for Oxygen Reduction Reaction, Chem. Rev. 116 (2016) 3594–3657. https://doi.org/10.1021/acs.chemrev.5b00462.

[213] J. Masa, W. Xia, M. Muhler, W. Schuhmann, On the Role of Metals in Nitrogen-Doped Carbon Electrocatalysts for Oxygen Reduction, Angew. Chem. Int. Ed. 54 (2015) 10102–10120. https://doi.org/10.1002/anie.201500569.

[214] A. Ōya, S. Ōtani, Catalytic graphitization of carbons by various metals, Carbon. 17 (1979) 131–137. https://doi.org/10.1016/0008-6223(79)90020-4.

[215] F.J. Maldonado-Hódar, C. Moreno-Castilla, J. Rivera-Utrilla, Y. Hanzawa, Y. Yamada, Catalytic Graphitization of Carbon Aerogels by Transition Metals, Langmuir. 16 (2000) 4367–4373. https://doi.org/10.1021/la991080r.

[216] M. Sevilla, A.B. Fuertes, Catalytic graphitization of templated mesoporous carbons, Carbon. 44 (2006) 468–474. https://doi.org/10.1016/j.carbon.2005.08.019.

[217] C.W.B. Bezerra, L. Zhang, K. Lee, H. Liu, A.L.B. Marques, E.P. Marques, et al., A review of Fe–N/C and Co–N/C catalysts for the oxygen reduction reaction, Electrochimica Acta. 53 (2008) 4937–4951. https://doi.org/10.1016/j.electacta.2008.02.012.

[218] U.I. Kramm, J. Herranz, N. Larouche, T.M. Arruda, M. Lefèvre, F. Jaouen, et al., Structure of the catalytic sites in Fe/N/C-catalysts for O2-reduction in PEM fuel cells, Phys. Chem. Chem. Phys. 14 (2012) 11673. https://doi.org/10.1039/c2cp41957b.

[219] T. Asset, P. Atanassov, Iron-Nitrogen-Carbon Catalysts for Proton Exchange Membrane Fuel Cells, Joule. 4 (2020) 33–44. https://doi.org/10.1016/j.joule.2019.12.002.

[220] S. Pérez-Rodríguez, D. Sebastián, C. Alegre, T. Tsoncheva, N. Petrov, D. Paneva, et al., Biomass waste-derived nitrogen and iron co-doped nanoporous carbons as electrocatalysts for the oxygen reduction reaction, Electrochimica Acta. 387 (2021) 138490. https://doi.org/10.1016/j.electacta.2021.138490.

[221] S. Kattel, G. Wang, A density functional theory study of oxygen reduction reaction on Me–N4 (Me = Fe, Co, or Ni) clusters between graphitic pores, J. Mater. Chem. A. 1 (2013) 10790. https://doi.org/10.1039/c3ta12142a.

[222] L. Qin, New Synthesis route of Iron-Based Catalyst for Electrochemical Oxygen Reduction Reaction, Int. J. Electrochem. Sci. (2020) 9168–9178. https://doi.org/10.20964/2020.09.26.

[223] Z. Yang, J. Wu, X. Zheng, Z. Wang, R. Yang, Enhanced catalytic activity for the oxygen reduction reaction with co-doping of phosphorus and iron in carbon, J. Power Sources. 277 (2015) 161–168. https://doi.org/10.1016/j.jpowsour.2014.12.018.

[224] Y. Hu, J.O. Jensen, W. Zhang, L.N. Cleemann, W. Xing, N.J. Bjerrum, et al., Hollow Spheres of Iron Carbide Nanoparticles Encased in Graphitic Layers as Oxygen Reduction Catalysts, Angew. Chem. 126 (2014) 3749–3753. https://doi.org/10.1002/ange.201400358.

[225] D. Wang, J. Hu, J. Yang, K. Xiao, S. Liang, J. Xu, et al., Fe and N co-doped carbon derived from melamine resin capsuled biomass as efficient oxygen reduction catalyst for air-cathode microbial fuel cells, Int. J. Hydrog. Energy. 45 (2020) 3163–3175. https://doi.org/10.1016/j.ijhydene.2019.11.201.

[226] J. Yang, J. Hu, M. Weng, R. Tan, L. Tian, J. Yang, et al., Fe-Cluster Pushing Electrons to N-Doped Graphitic Layers with Fe_3C(Fe) Hybrid Nanostructure to Enhance O_2 Reduction Catalysis of Zn-Air Batteries, ACS Appl. Mater. Interfaces. 9 (2017) 4587–4596. https://doi.org/10.1021/acsami.6b13166.

[227] D. Thanh Tran, T. Kshetri, N. Dinh Chuong, J. Gautam, H. Van Hien, L. Huu Tuan, et al., Emerging core-shell nanostructured catalysts of transition metal encapsulated by two-dimensional carbon materials for electrochemical applications, Nano Today. 22 (2018) 100–131. https://doi.org/10.1016/j.nantod.2018.08.006.

[228] X. Liu, I.S. Amiinu, S. Liu, K. Cheng, S. Mu, Transition metal/nitrogen dual-doped mesoporous graphene-like carbon nanosheets for the oxygen reduction and evolution reactions, Nanoscale. 8 (2016) 13311–13320. https://doi.org/10.1039/C6NR03247H.

[229] Z. Liu, Z. Li, J. Ma, X. Dong, W. Ku, M. Wang, et al., Nitrogen and cobalt-doped porous biocarbon materials derived from corn stover as efficient electrocatalysts for aluminum-air batteries, Energy. 162 (2018) 453–459. https://doi.org/10.1016/j.energy.2018.07.175.

[230] Z. Liang, H. Zheng, R. Cao, Recent advances in Co-based electrocatalysts for the oxygen reduction reaction, Sustain. Energy Fuels. 4 (2020) 3848–3870. https://doi.org/10.1039/D0SE00271B.

[231] C. Du, H. Huang, X. Feng, S. Wu, W. Song, Confining MoS_2 nanodots in 3D porous nitrogen-doped graphene with amendable ORR performance, J. Mater. Chem. A. 3 (2015) 7616–7622. https://doi.org/10.1039/C5TA00648A.

[232] R. Cheng, J. Yang, M. Jiang, A. Dong, M. Guo, J. Zhang, et al., Hierarchical Porous Manganese- and Nitrogen-Codoped Carbon Nanosheets Derived from Surface Modified Biomass as Efficient Oxygen Reduction Catalysts for Al-Air Batteries, J. Electrochem. Soc. 167 (2020) 110552. https://doi.org/10.1149/1945-7111/aba5da.

[233] C. Zheng, X. Zhang, Z. Zhou, Z. Hu, A first-principles study on the electrochemical reaction activity of 3d transition metal single-atom catalysts in nitrogen-doped graphene: Trends and hints, EScience. (2022) S2667141722000210. https://doi.org/10.1016/j.esci.2022.02.009.

[234] J. Zhang, Y. Wang, Y. Wang, M. Zhang, Catalytic Activity for Oxygen Reduction Reaction on CoN_2 Embedded Graphene: A Density Functional Theory Study, J. Electrochem. Soc. 164 (2017) F1122–F1129. https://doi.org/10.1149/2.1031712jes.

[235] X. Zhang, Z. Yang, Z. Lu, W. Wang, Bifunctional CoNx embedded graphene electrocatalysts for OER and ORR: A theoretical evaluation, Carbon. 130 (2018) 112–119. https://doi.org/10.1016/j.carbon.2017.12.121.

[236] B. Ni, L. Wu, R. Chen, C. Shi, T. Chen, Fe/Co-based nanoparticles encapsulated in heteroatom-doped carbon electrocatalysts for oxygen reduction reaction, Sci. China Mater. 62 (2019) 1626–1641. https://doi.org/10.1007/s40843-019-9476-5.

[237] J. Li, M. Chen, D.A. Cullen, S. Hwang, M. Wang, B. Li, et al., Atomically dispersed manganese catalysts for oxygen reduction in proton-exchange membrane fuel cells, Nat. Catal. 1 (2018) 935–945. https://doi.org/10.1038/s41929-018-0164-8.

[238] T. Sharifi, E. Gracia-Espino, A. Chen, G. Hu, T. Wågberg, Oxygen Reduction Reactions on Single- or Few-Atom Discrete Active Sites for Heterogeneous Catalysis, Adv. Energy Mater. 10 (2020) 1902084. https://doi.org/10.1002/aenm.201902084.

[239] H. Fei, J. Dong, Y. Feng, C.S. Allen, C. Wan, B. Volosskiy, et al., General synthesis and definitive structural identification of MN4C4 single-atom catalysts with tunable electrocatalytic activities, Nat. Catal. 1 (2018) 63–72. https://doi.org/10.1038/s41929-017-0008-y.

[240] W. Niu, J. He, B. Gu, M. Liu, Y. Chueh, Opportunities and Challenges in Precise Synthesis of Transition Metal Single-Atom Supported by 2D Materials as Catalysts toward Oxygen

Reduction Reaction, Adv. Funct. Mater. 31 (2021) 2103558.
https://doi.org/10.1002/adfm.202103558.
[241] J. Zhang, H. Yang, B. Liu, Coordination Engineering of Single-Atom Catalysts for the Oxygen Reduction Reaction: A Review, Adv. Energy Mater. 11 (2021) 2002473.
https://doi.org/10.1002/aenm.202002473.

Declaration of interests

☒ The authors declare that they have no known competing financial interests or personal relationships that could have appeared to influence the work reported in this paper.

☐The authors declare the following financial interests/personal relationships which may be considered as potential competing interests: